Vegetation responses to variations in climate: A combined ordinary differential equation and sequential Monte Carlo estimation approach

O.A. Bruzzone [*], D.V. Perri, M.H. Easdale

IFAB, CONICET/INTA, Modesta Victoria 4450, San Carlos de Bariloche, Rio Negro, Argentina

A B S T R A C T

Vegetation responses to variation in climate are a current research priority in the context of accelerated shifts generated by climate change. However, the interactions between environmental and biological factors still represent one of the largest uncertainties in projections of future scenarios, since the relationship between drivers and ecosystem responses has a complex and nonlinear nature. We aimed to develop a model to study the vegetation's primary productivity dynamic response to temporal variations in climatic conditions as measured by rainfall, temperature and radiation. Thus, we propose a new way to estimate the vegetation response to climate via a non-autonomous version of a classical growth curve, with a time-varying growth rate and carrying capacity parameters according to climate variables. With a Sequential Monte Carlo Estimation to account for complexities in the climate-vegetation relationship to minimize the number of parameters. The model was applied to six key sites identified in a previous study, consisting of different arid and semiarid rangelands from North Patagonia, Argentina. For each site, we selected the time series of MODIS NDVI, and climate data from ERA5 Copernicus hourly reanalysis from 2000 to 2021. After calculating the time series of the a posteriori distribution of parameters, we analyzed the explained capacity of the model in terms of the linear coefficient of determination and the parameters distribution variation. Results showed that most rangelands recorded changes in their sensitivity over time to climatic factors, but vegetation responses were heterogeneous and influenced by different drivers. Differences in this climate-vegetation relationship were recorded among different cases: (1) a marginal and decreasing sensitivity to temperature and radiation, respectively, but a high sensitivity to water availability; (2) high and increasing sensitivity to temperature and water availability, respectively; and (3) a case with an abrupt shift in vegetation dynamics driven by a progressively decreasing sensitivity to water availability, without any changes in the sensitivity either to temperature or radiation. Finally, we also found that the time scale, in which the ecosystem integrated the rainfall phenomenon in terms of the width of the window function used to convolve the rainfall series into a water availability variable, was also variable in time. This approach allows us to estimate the connection degree between ecosystem productivity and climatic variables. The capacity of the model to identify changes over time in the vegetation-climate relationship might inform decision-makers about ecological transitions and the differential impact of climatic drivers on ecosystems.

1. Introduction

Ecosystem responses to climatic variability are a major research priority in the context of accelerated shifts generated by climate change (Walther et al., 2002). In particular, it is widely accepted that vegetation is exposed to increasing environmental and meteorological conditions variation, involving extreme events such as flooding (Arnell and Lloyd-Hughes, 2014; Poff, 2002) and long-lasting unfavourable circumstances as in the case of droughts (Cook et al., 2018; Pokhrel et al., 2021),

threatening their survival. Grassland ecosystems will likely experience the greatest proportional change in biodiversity because of the substantial influence of biodiversity change drivers such as land-use change, climate change, nitrogen deposition, biotic exchange and elevated carbon dioxide concentration (Sala et al., 2000). However, the interactions among physical and biological factors still represent one of the largest uncertainties in projections of future scenarios, since the relationship between drivers and ecosystem responses has a complex and nonlinear nature (Walther, 2010). Then, the nature of the relationship among

---

factors, the parameter estimations and the magnitude of the ecosystem response to drivers are still major research topics in such complex systems (Moore, 2018).

Physiological and ecosystem responses to climatic variables or, more generally, to varying environmental conditions, have several levels of complexity. The effect of temperature is not monotonic, under both field and laboratory conditions, the photosynthetic activity of vegetation response increases with temperature, and after reaching a maximum decreases again (e.g. Varela et al., 2012), and similar non-monotonic patterns were found for vegetation response to rainfall with productivity increases, and then decreasing after reaching optimal values (Zhang et al., 2020). Such a response is common in most ectothermic organisms, and several nonlinear models of physiological response to temperature were developed (Logan et al., 1976; Sharpe and DeMichele, 1977; Briere et al., 1999). However, the response to rainfall is more complex, according to the two-layer hypothesis (Walter, 1939, 1971; Ward et al., 2013). In arid and semiarid ecosystems, water use is partitioned depending on the niche dimension: grasses and other herbaceous plants use the water available in the upper layers of soils and shrubs use water from the lower layers. This pattern was identified in different regions (Ward et al., 2013), including the Patagonian steppes from Argentina (Pelaez et al., 1994; Sala et al., 1989; Soriano and Sala, 1984). However, the latter is not a strict separation, thus some shrubs also use water from the upper layers (Pelaez et al., 1994). By developing roots that grow deep, shrubs reach lower layers of soil. Consequently, some shrubs have access to water from distant sources such as groundwater, which can flow from long distances within the basin, generating a water availability pattern that is delayed and low-pass filtered (i.e. a smoothed function with the high-frequency variability dampened or removed) rainfall function (Crosbie et al., 2005; Oudin et al., 2004; Sun and Wang, 2012; Wu et al., 2002). The said pattern is also a common strategy for other plants, even for herbaceous species, which live in the neighbourhood of shrubs or within a wetland. Hence, they use the water table whose dynamics are also dependent on the basin geomorphology.

In biological organisms, the interaction among different resources follows Liebig's *Law of Minimum* (Liebig et al., 1842; Hooker Jr, 1917). From that perspective, the growth is not a function of the total available resources, but of the scarcest or lacking resources. Therefore, it is known as the *limiting factor*. The law of the minimum in non-stationary systems or systems being forced to change by the effect of an external driver, such as semiarid ecosystems under the effect of climate change, has complex implications (Easdale et al., 2022). In particular, a non-linear response is induced when the resource is limited, so the system will increase its output (or productivity) until another resource becomes limited (following a sigmoidal response in the process). For example, if an ecosystem is limited by water, it will increase its productivity with increasing amounts of water until it becomes limited by temperature or nutrients. Hence, a methodology capable of dealing with changes in the limiting factors is a desirable tool in the analysis of the long-term dynamics of ecosystems.

The approaches aimed at tackling the vegetation response to variations in climate range from very simple—such as those based on linear regressions—to highly complex models formulated as complex spatially-explicit dynamical systems. As in the mathematical modelling literature, these approaches are subject to a trade-off between biological meaning and parameterization adjustment (Jehn et al., 2019). On the one hand, the simpler models lack biological realism but the parameters are easier to calculate. On the other hand, more complex models are closer to emulating biophysical realism, but their parameters are difficult to estimate due to their greater number and nonlinearity and lack of generality because these are more case-specific (Sharov, 1996), and more prone to overfitting (Claeskens and Hjort, 2008). Very simple models might lead to incorrect results as a consequence of linearizing nonlinear relations, do not adequately approximate real biophysical processes (eg: water use by vegetation), or because they ignore temporal autocorrelations in data; whereas more complex models may result in uncertain

predictions due to the high dimensionality of the error matrix and given the same data set, to the decrease in degrees of freedom of the model, increases the uncertainty of the estimation, for example, for dynamical systems, the logarithm of the error decreases with the logarithm of the degrees of freedom of the model (Mitchell, 2015). Therefore, a combination of a model with biological realism and simple calculations is more desirable when using field data.

Resolution issues also compromise the modelling of ecological processes. As the complexity of the studied system increases with the temporal resolution, for example, according to the central limit theorem, the standard deviation of an independent sampled random variable decreases with the square root of the sample size (Rosenblatt, 1956). Lower-resolution studies usually group together several consecutive samples, in a procedure known as data decimation or downsampling, reducing also the temporal variability. Reducing the resolution also increases the aliasing in the time series (Landau, 1967), resulting in series that contain less information and are also distorted, so keeping the original resolution is a desirable property of any analysis of a time series data. This is very usual in climate-vegetation studies, which are performed at a one-year or interannual time resolution (e.g. Hou et al., 2015; Luo et al., 2020), and less frequent in higher than annual resolution (Roerink et al., 2003). While the main advantage of using decimated time series is the possibility of using simultaneous meteorological and vegetation data, it can be improved by using time-lag models (Wu et al., 2015).

With no seek of completeness, some approaches found in the literature are soil-plant-climate biophysical models (Johnson et al., 2008; Jones et al., 2003), multiple linear regression and factor analysis on yearly aggregated data (Çamdevýren et al., 2005), stepwise cluster analysis (Zheng et al., 2018), harmonic and Fourier analysis (Menenti et al., 2010), and distributed-delay models with Gaussian process (Bruzzone and Easdale, 2021; Díaz-Villa et al., 2022).

An alternative option is to use simple dynamical models based on ordinary differential equations (ODE), frequently used to explore relationships among different variables (Rosenbaum and Rall, 2018; Strohm and Tyson, 2012). The development is conceived from a bottom-up logic aimed at describing dynamical systems. The study of plant population or productivity dynamics has a long historical tradition, it was performed even before the availability of the first time series of vegetation indexes in the 1980s, as in Noy-Meir's theoretical models (Noy-Meir, 1973, 1975). However, one main drawback of this approach is that if the parameters are fixed, the system is assumed to be time-invariant, which means that the response to a variation on external conditions is the same with time, and differences between measurements and expected values are attributed to measurements errors and model uncertainty, as in the case of Kalman filters (Kalman, 1960). Examples are the application to time series of NDVI, EVI or other remote-sensed vegetation data of Linear and Non-Linear Time Invariant (LTI and NLTI, respectively) filter as in Kogan and Zhu, (2001), and more frequently, several versions of the Kalman Filters (Kleynhans et al., 2010; Sedano et al., 2014).

Other less-explored alternatives are non-autonomous versions of classical population dynamic models with time-varying parameters that were first proposed by Coleman (1979) (see Hallam and Clark, 1981), which are simple yet powerful alternatives. In these models, the parameters are allowed to vary over time according to some external variable, hence the "non-autonomous" name, while the others in which the parameters are fixed and are not influenced by external factors are called "autonomous". In these cases, the complexities of the physiological, soil and other environmental components are replaced by black-box population-level functions that modify the model parameters, resulting in a simple model configuration. These kinds of models are adequate to describe biological systems in which the population response lags behind changes in the environmental conditions (Baranyi et al., 1993a). Some examples applied to different types of biological populations are Ikeda and Yokoi (1980) for fishes, Baranyi et al. (1993a, 1993b) for

bacterial growth, Bruzzone and Utgés (2022) for insects, and Samanta (2012) for modelling population dynamics in environments subject to pollution.

Therefore, instead of developing a high-intrinsic-complexity model where the variability of the vegetation response to climate is modelled in detail, designing a hybrid approach where model parameters are allowed to vary over time instead of being fixed and invariant is an alternative. This procedure reduces the requirements of data details—-which are frequently unavailable or difficult to obtain—and avoids using a huge number of parameters which increases the uncertainty of the estimations.

Another issue concerning the vegetation response to climate variations is tracking the studied phenomenon variations through time. That is usually accomplished via Granger causality (Granger, 1969; see Kaufmann et al., 2003, de Jong et al., 2011). The main drawback of the Granger Causality—as originally formulated via autoregressive models is its linearity when analyzing strongly nonlinear systems such as climate vegetation or most biological systems (Diks and Wolski, 2016). Hence, for these cases, nonlinear versions are also proposed (Papagiannopoulou et al., 2017), whereas an alternative is to use a model-based method with differential equations (Friston et al., 2013).

Since most natural systems are highly complex—and the relationship between ecosystems and climate is not an exception—a compromise solution is still needed. In the context of this research, we tackle variations by using a simple parametric model between time-varying environmental variables (i.e. climate) and population-level parameters (i.e. productivity of ecosystems), without increasing the complexity of the model. Several alternatives are available in the literature for this kind of situation. For instance, one option is to locally fit the model over a sliding window on the data time series. This approach has two main

methodology families: i) Moving Horizon Estimation (Rawlings, 2009; Hedengren et al., 2014), which is itself a generalization of the Kalman Filter (Rao et al., 2003); and ii) Particle Filter or Sequential Monte Carlo Estimation (hereafter named SME), which is a bayesian-based methodology that sequentially implements a Markov Chain Montecarlo (MCMC) procedure on the data (Del Moral, 1996). SME has already been used by several authors for modelling NDVI time series with sound results (Chakraborty et al., 2017; De Bernardis et al., 2016a, 2016b).

We propose the combination of SME methods with non-autonomous models to address the shortcomings of both types of methodologies, and to account for the model uncertainties and measurement errors, while simultaneously modelling variation on the model parameters in response to external factors. Therefore, in this study, we aimed at developing a model to study the dynamic response of vegetation primary productivity to temporal variations in climatic conditions as measured by rainfall, temperature and radiation. In particular, how the relationship between climatic drivers and vegetation responses varies over time and the coupling strength among them. The questions that guided this research were: i) does the ecosystem productivity respond differently under varying climatic conditions over time? ii) Can the ecosystems couple and decouple from climatic drivers over time? We proposed the application of a simple ODE-based dynamical system based on a non-autonomous version of the well-documented Brody-monomolecular growth curve with a time-varying carrying capacity. We added a Sequential Monte Carlo Estimation applied to a moving window to account for the model parameter's variation over time and the overall explanatory power of the model.
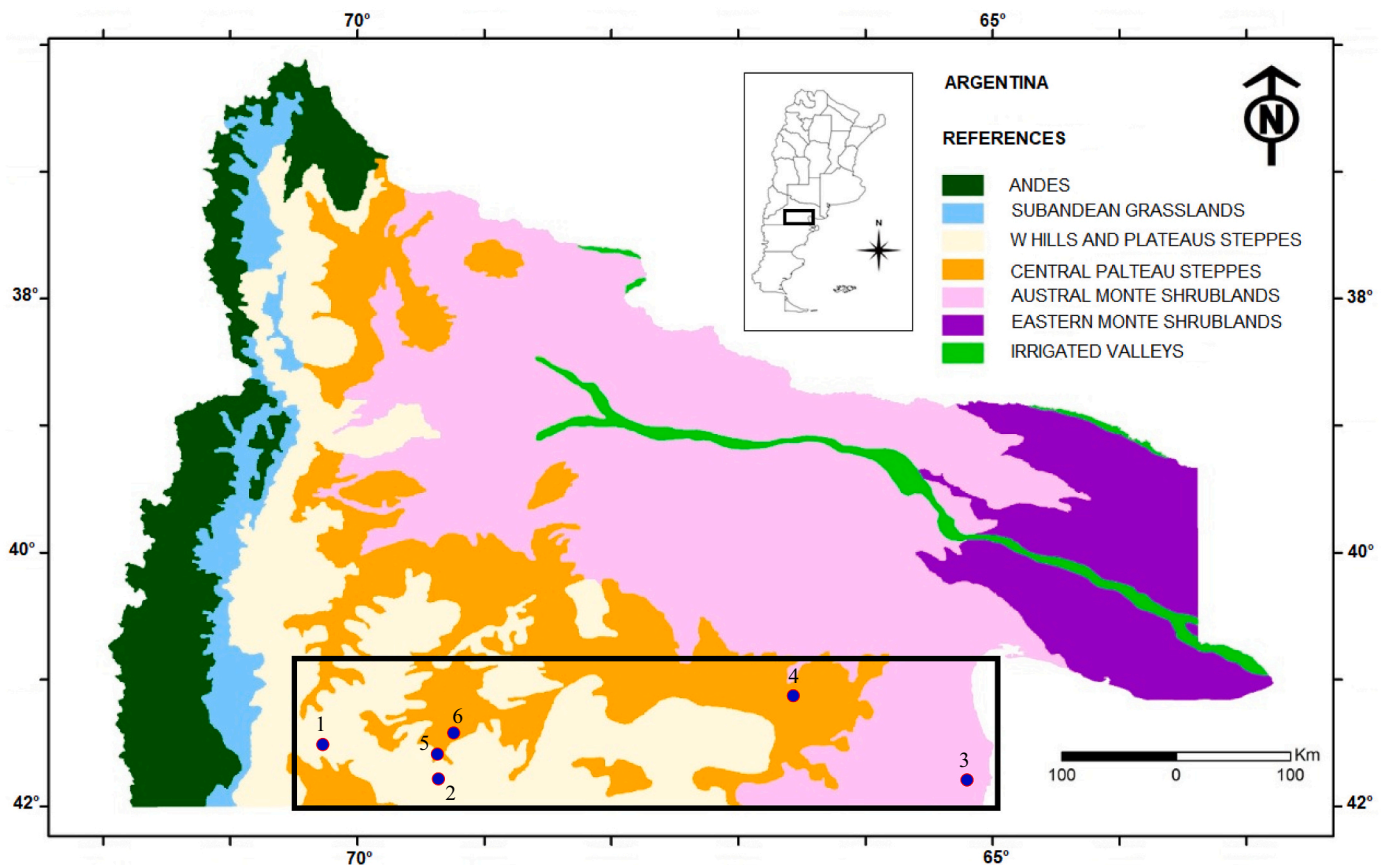

Fig. 1. Map of the study area, located in the Rio Negro Province, Argentina, showing the principal ecosystem types in different colours. Red-blue circles are the geographical position of the archetypoid pixels used in this study, and the adjacent number indicates the archetype number, according to Table 1. (For interpretation of the references to colour in this figure legend, the reader is referred to the web version of this article.)

2. Materials and methods

2.1. Study cases

The study area was the arid and semiarid rangelands of North Patagonia, Argentina (see map in Fig. 1). This area is characterised by shrublands and shrub-grass steppes, with small areas of meadows towards the west. Climate is arid and cold, with a W-E rainfall gradient of 250 mm to 150 mm, and mean annual temperatures varying spatially between 8 °C and 13 °C, at the upper and lower heights, respectively (Godagnone and Bran, 2009). Altitude decreases from the west (with hills and plateaus over 1000 m.a.s.l.) to the east and northeast (with great plains below 500 m.a.s.l.).

We used six previously identified sites that best represented different rangeland dynamics in a great semiarid region from North Patagonia, Argentina (Bruzzone and Easdale, 2021). In that study, an archetypal analysis was applied to a matrix containing the power spectrum of the MODIS NDVI time series of a wide region, considering the above-mentioned east-west environmental gradient. Six pixels—named quasi-archetype pixels—represented key areas with contrasting dynamics, whose linear combination explained 97% of the power spectrum variability in the studied area (see geographical location and main environmental characteristics in Table 1 and Fig. 2). Hence, the different pixels are both contrasting in their temporal dynamics and representative of large areas of similar rangeland dynamics. This region has a low human population density and its main economic activity is extensive livestock production and pastoralism (Easdale et al., 2009). Therefore, it is a large area with low human intervention, where vegetation cover was less modified as compared with land-use change involving cover shifts (e.g. agriculture, irrigation or mining). Then, for the 20-year period analyzed in this study, rangeland dynamics were mostly driven by climate and environmental factors at a regional scale.

2.2. Data source

For each pixel, we obtained the time series of the Normalised Difference Vegetation Index (NDVI) from the Moderate Resolution Imaging Spectroradiometer dataset (MODIS13Q1, version 6). The spatial resolution of the pixel is 6.25 ha and the series consisted of 16-day composites for the period February 2000 to September 2021. Time series from these pixels were processed by removing the negative values and by only keeping the positive values, whose pixel reliability index was 0 or 1. The others were marked as invalid data and removed from the analysis.

In order to keep the resolution of the study at the highest level, we used a single pixel for each analysis, instead of pooling several neighbouring pixels into a single time series. Pooling neighbouring pixels will increase the uncertainty on the estimation parameters by mixing more different vegetation types. In addition, since it is a mountainous region,

the presence of topographical differences between pixels from the same ecosystem may produce differences in the time delay of underground water availability, which distort the window function used to model water availability in unpredictable ways. Finally, by using a single pixel we avoid causing information loss by jitter (or phase noise), caused by the topographical differences among pixels.

For the explanatory variables, climate data were obtained from the ERA5 hourly reanalysis dataset (Hersbach et al., 2020). These ERA5 data have a spatial resolution of 31 km, and the hourly data were aggregated into daily data, so the final temporal resolution was 24 h. We selected the cell from the 31 km dataset matrix that most overlapped with each MODIS pixel. The selected meteorological variables that were used for the analysis were: i) 2-m temperature, ii) total precipitation and iii) total surface radiation, for the period 1998 to 2021.

2.3. Model formulation

We used a non-autonomous growth curve as the base for the model development. In the study resolution timescales—which was the mean distance in time between two consecutive MODIS images (16 days)—we expected to find a phenological rather than a populational response. Hence, instead of the more population-oriented Sigmoid curves, such as Gompertz or logistic models, we chose a physiological-type model, without inflexion points. The reason for this choice is that a population model has, firstly, an exponential growth, and then the growth slows down following a typical sigmoidal shape. Due to the temporal resolution of this study (16 days), the population response is very small, and the plants present in the MODIS images are growing or reducing their aerial parts (mostly leaves) in response to changing environmental conditions. Therefore, the response is not necessarily expected to be sigmoidal. Following the model from Zeng et al. (2002), we used a well-known and simple vegetation dynamics model, which is also similar to the basic formulation of the monomolecular growth curve and the Michaelis-Menten enzyme kinetics model, which is one of the best-known models of this type and the basis of many physiology models. Therefore as a starting point, we used the following differential equation:

$$dN(t)/dt = r\left(K_c(t) - N(t)\right) \tag{1}$$

where N is the vegetation activity, represented by the NDVI, r is the growth rate or speed of the vegetation response to a change in the environmental conditions, and K_c or carrying capacity is the expected photosynthetic activity under the given set of c climatic conditions. In this curve, the resulting growth is the multiplication of the growth rate by the difference between the actual population size (N) and the carrying capacity (K). Therefore, under this model, if $K_c > N$ it results in a positive growth and the photosynthetic activity increases towards K_c; also, if $K_c < N$, the growth is negative, meaning that the photosynthetic

Table 1
List of geographical coordinates and main environmental characteristics of the six quasi-archetype pixels of MODIS used in this study, which represent the different rangeland archetypes, respectively. Quasi-archetype data and main features were obtained from Bruzzone and Easdale (2021).

| Archetype #	Latitude	Longitude	Main ecosystem features	Height (m. a.s.l.)	Mean Daily Temperature (°C)	Mean Daily Radiation J /m²	Mean Annual Rainfall (mm)
1	−41° 31′ 22.50"	−70° 17′ 1.73"	Highlands and lagoons with stochastic dynamics	1374	6.6	13.6	487.2
2	−41° 47′ 52.50"	−69° 22′ 28.41"	Rangelands in negative phase	1140	12.4	13.2	425.1
3	−41° 48′ 30.00"	−65° 12′ 46.46"	Oscillatory shrublands	168	16.6	12.2	874.3
4	−41° 8′ 0.00"	−66° 34′ 23.56"	Shrublands with a shoulder-head-shoulder temporal pattern	790	16.4	12.8	680.6
5	−41° 35′ 37.50"	−69° 23′ 9.23"	Stationary meadows	977	12.8	13.2	448.5
6	−41° 26′ 0.00"	−69° 15′ 1.01"	Post-perturbation recovery of lowland steppes	911	14.1	13.4	386.1
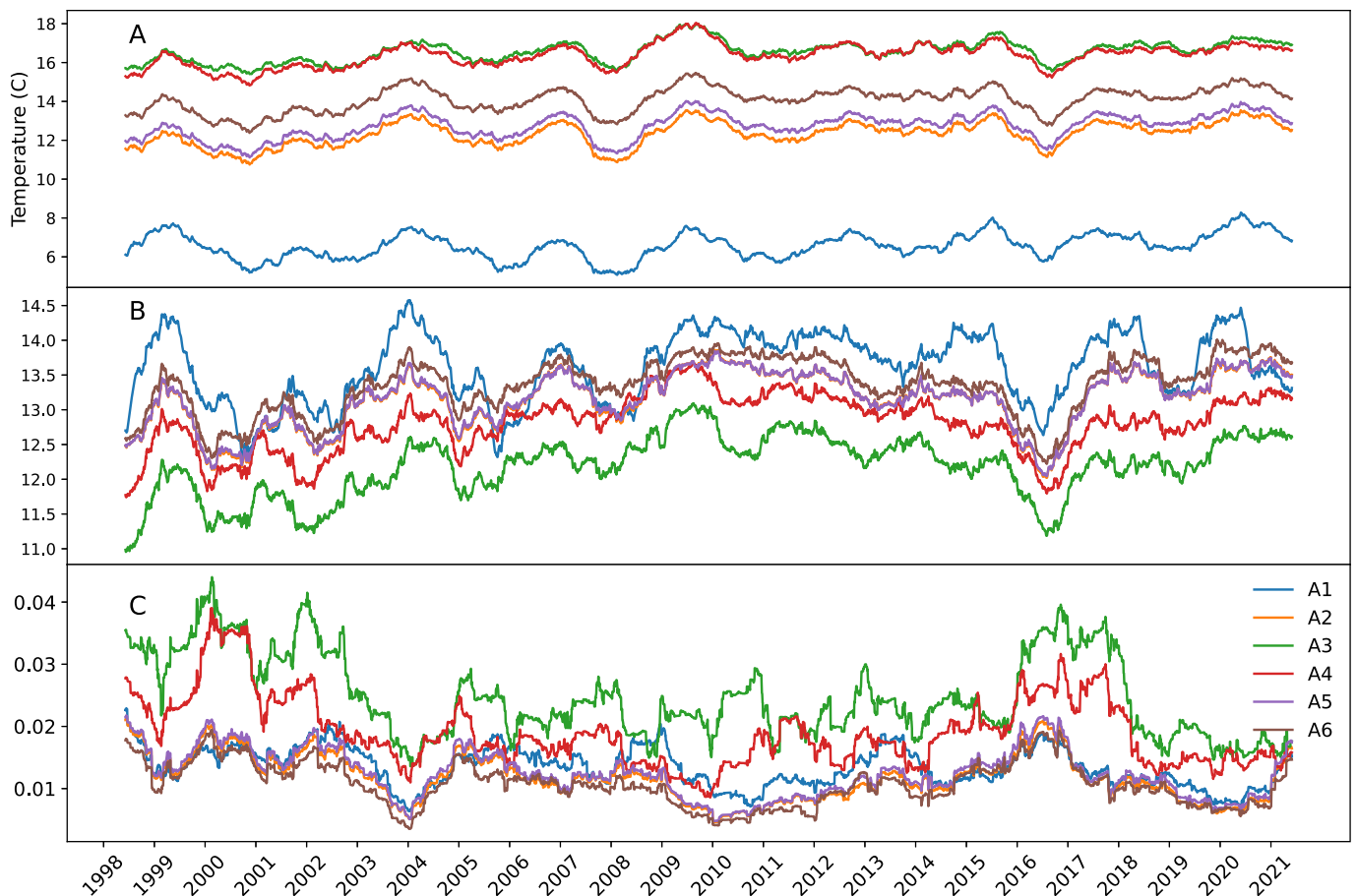
Fig. 2. Annual moving averages of temperature (A), radiation (B), and rainfall (C) for the six studied quasi-archetype pixels. Source of data: ERA5 reanalysis data set (Herbach et al., 2020).

activity decreases. The model is simply a growth curve with a time-varying carrying capacity. Under constant conditions, K_c is the asymptotic value of N (or NDVI), having the same units (unitless in this case), but here, K_c is allowed to freely vary according to the climate, so it is a non-autonomous model, as one of the parameters varies according to one external variable. Hence, the vegetation response to climate was measured by the variation of the K parameter. If K increased, the N variable increased following that parameter at a rate of r. As a consequence, r is the rate of increase, but also the inverse of the vegetation response time to the climate in years (y), according to the model of Zeng et al. (2002), having thus units of $1/y$.

Vegetation was assumed to respond to three climatic variables: i) mean daily temperature (T), ii) daily rainfall (P), and iii) mean daily radiation (R). In all cases, we assume that the carrying capacity K responds logistically to changes in climate because NDVI on land is a 0 to 1 bounded variable, thus it cannot have expected values outside that interval. So, for any climatic variable, K is:

$$K_c(t) = 1 - \frac{1}{1 + e^{-c(t)}} \qquad (2)$$

where c can be any climatic variable (either T, P or R) and c(t) is its time-series. Hence, for K dependent on temperature, K is K_T, for K dependent on rainfall is K_P, and if it depends on radiation is K_R.

Since rain is a highly concentrated phenomenon in time, with most of the days without precipitation, using it will directly lead to a time series with most of the estimated K being zeros. Therefore, we created a *water availability* function which is the integral of a water balance function into the time series multiplied by the rainfall in that period, transforming eqs. 1 and 2 into an integrodifferential equation. That function is the

convolution between the rainfall as a function of time and a probability density function that smooths the rainfall time series. A probability distribution function is chosen to avoid inflating or deflating artificially the estimated water availability and the weighting function must have a constant integral equal to one. As a result, the water availability is a weighted moving average of the rainfall data. Thus, the water availability is defined as follows:

$$w(t) = \int_{x=t}^{x=t-d} P(t)G(x, \alpha, \theta)dx \qquad (3)$$

where t is the time, w the available water for the plants at time t, $P(t)$, the rainfall, d the time scale at which the water availability operates, x the number of days to the past at which the w function is evaluated, and G is a probability density function of a general gamma statistical distribution with parameters α (shape) and θ (scale). Following Bain and Engelhardt (1992), to avoid confusion with the parameter K from eqs. 1 and 2, we called the shape parameter α, instead of κ, as is usual in shape and scale representations of this statistical distribution. While previous studies have chosen simple moving averages for modelling this variable, that function together with the usage of a square-shaped window results in the same weight as rainfall episodes occurring closer in time to the NDVI measurement data and several weeks after.

On the other hand, with that statistical distribution, we modelled the process of charging and slowly discharging the water reservoir afterwards. In the case of superficial water reservoirs, that is moisture present in the superficial layers of soil that only recharge from rainfall and do not receive water from underground reservoirs or runoff from areas located in topographically higher altitudes, the moisture discharge process usually resembles an exponential decay function (e.g.

Nakanwagi et al., 2020; Xu et al., 2004), and is a consequence of the "soil as a capacitor" model proposed by Bisigato et al. (2013). As the exponential decay process is a special case of the gamma curve, it can be also modelled using that curve. While other options are possible, we chose that statistical distribution because it is a simple and straightforward description of the rainfall accumulation process, and it is frequently used to model accumulated rainfall processes (Yoo et al., 2005; Husak et al., 2007; Martinez-Villalobos and Neelin, 2019). Another advantage according to Martinez-Villalobos and Neelin (2019) is that it makes it possible to track distribution changes quantitatively. Gamma distribution is also used to convolve the rainfall time series to estimate groundwater level recharge (Besbes and De Marsily, 1984; Collenteur et al., 2019).

While an important discharge rate might depart the process from that modelled via a Gamma curve, it is negligible in the semi-arid conditions of most of the study area. Hence, for the purposes of our study, a convolved vector between a rainfall time series and a Gamma distribution curve is assumed to account for the whole process of water charge (via rainfall or underwater movement), and depletion (via plant usage, evaporation and discharge), measured at the centre of the archetypoid pixel, without the use of a complex water balance model.

Therefore as explained above, to solve the eq. 3 model, the series was filtered via convolution of the rainfall time series and by using a Gamma distribution, resulting in an estimated *water availability* time series. The model was defined as follows:

$$w = P * G(\alpha, \theta) \tag{4}$$

w being the water availability function, G the same Gamma distribution used in eq. 3. Then K_P is replaced by K_w, to denote its dependence on water availability, which has an indirect dependence on rainfall.

2.3.1. Interaction among variables

The interaction among variables has a complex nature and solutions are not trivial. Some alternatives, such as multiple linear or polynomial models, can produce absurd results such as in the case of a humid winter, where sub-zero temperatures predict zero aboveground productivity (or $K(t) = 0$), but a simultaneous abundant water availability predicts high productivity ($K(t) >> 0$). In these circumstances, an additive linear model will have an output that is a weighted average between what is expected under the influence of both the temperature and the rainfall. Even with more complex models —such as multi-polynomial ones—- there is still the possibility that under extreme conditions the $K(t)$ is higher than zero.

As a consequence, we decided to choose the simplest model that complies with Liebig's *Law of Minimum* (Liebig et al., 1842). This model has a restriction: the expected value produced must be zero if the conditions in at least one variable are below a certain value in which the plants are physiologically unable to produce any outcome (i.e. aboveground productivity zero or near-zero). For example, if there is zero water availability, the roles of radiation or of temperatures are not relevant, since the productivity must be zero. As well, if the temperature is too low, the plants will remain dormant, independent of water availability or radiation levels.

Two simple models comply with this condition: a) the minimum and b) the multiplicative. The minimum simply chooses the lowest of a series of proposed values and the multiplicative their multiplication. For example, if the expected K values under the three chosen variables are 0.1, 0.5, and 0.4, the result will be 0.1 under the minimum model and 0.02 under the multiplicative model. Also, if any of the expected K values is zero, the final expected K will also be zero, by modelling the dynamics of a system with a limiting resource. In Díaz-Villa et al. (2022), the minimum model was slightly better than the multiplicative one in fitting the dynamics of an EVI vegetation index of a subtropical forest. However, in the preliminary analyses, we found that it was very difficult to make it fit with the approach used in this paper. Therefore, following

Bruzzone and Easdale (2021), we choose the multiplicative model. With this model—as in NDVI—all the expected K values as a function of climate range between zero and one, so the multiplication is the same as multiplying proportions. If the rainfall produces a 0.1 level, temperature 0.5, and radiation 0.4, the interpretation is that temperature produces an expected value of one-fifth of the maximum possible 0.1, instead of 1. That logic has a more biological sense as compared to an arbitrary polynomial model, which can be used as an alternative.

In this study area, the arid and semiarid rangelands periodically experience droughts and low and very high-temperature conditions, which become constraints for the development of vegetation, even if the other resources are abundant (Bruzzone and Easdale, 2021; Jobbágy et al., 2002). The usage of a multiplicative model allowed us to simplify the modelling of species distribution and abundance in which the resources become limited (Persson et al., 2007; Vaz et al., 2008; McCune, 2011). Since the biological meaningful NDVI values range between 0 and 1 (the negative values meaning bare soil, water bodies or snow cover), the use of a multiplicative relation allows for estimating the limiting resource. Hence, the K depending on climate (K_c) is then a multiplication of the estimation of the three K estimated using individual climatic variables.

$$K_c(t) = K_T(t) K_R(t) K_w(t) \tag{5}$$

2.3.2. Full model

The expected NDVI value is the model in eq. (1), with the $K_c(t)$ term replaced by eq. 5—which in turn contains eq. 4—into the $K_w(t)$ term of eq. 5. Hence, we assume that $N(t)$ is the central value of a stochastic process in which the measured *NDVI* value is the sum of N and a Gaussian error term containing the measurement errors:

$$NDVI(t) = N(t) + \varepsilon(t) \tag{6}$$

with

$$\varepsilon(t) \sim N(0, \sigma(t))$$

where *NDVI(t)* is the measured NDVI value at time t and $\varepsilon(t)$ is the error term at time t which follows a Normal distribution with mean zero and standard deviation σ. The standard deviation varies with time, allowing an increase (or decrease) of error with time. For the sake of simplicity, we assume that the errors are purely additive (i.e. do not change with N). Finally, we assume that all the autocorrelation measurements are caused by the underlying deterministic process N, so the errors $\varepsilon(t)$ are independent. In this way, we avoid using an ARIMA or a Gaussian process in the model.

NDVI is a constrained variable, defined in the interval $[-1,1]$. Although, as mentioned above, only the values between 0 and 1 have biological meaning, there are certainly negative measured values, and very low values are noise caused by reflections of bare soil and snow cover. The $\varepsilon(t)$ term allows us to model the stochastic process for which there is some NDVI variability, even though N is low or even zero, leading to a better estimate of the process variability and modelling errors.

The full formulation of the model contained a total of ten parameters, the growth rate (r), the origin and slope of the logistic function of K as a function of the three climate variables (T_o, T_{sl}, R_o, R_{sl}, W_o, W_{sl}), the α (shape) and θ (scale) of the Gamma function, and finally, the standard deviation (σ) of the error function. For the Gamma function, to ease the interpretation, the mean and standard deviation are called here PP_{Delay}, and PP_{width} respectively, and were calculated from α and θ, as the mean time from the rainfall and standard deviation are more intuitive indicators of the properties of the distribution than its original parameters.

2.4. Numerical methods

To estimate the parameters of the proposed model and its variation

over time, we chose a fully Bayesian approach in a sequential way, by a method called particle filter.

2.4.1. Particle filter

The objective of this analysis is to estimate the internal state and the model parameters described in eqs. 1 to 6, given a series of noisy measurements in the NDVI time series. Under this procedure, the Bayesian process of choosing a priori distribution, and using it to draw random values via a Montecarlo algorithm to generate posterior estimations of the parameters, is done sequentially and recursively along the time series. Hence, the posterior distribution from one step is the prior distribution of the following. As a result, the estimations are obtained in the form of a posteriori distribution of the state variable and model parameters across time. The internal state is represented solely by the estimated N value, the parameters are the inverse of response time r, the variables that compose the three Kc models, and the standard deviation of the error term. All the parameters are considered to be variable with time, or its posterior distribution is not constant in time as a consequence of some unknown physical process to be inferred after analyzing the model posterior distributions time series.

To measure the vegetation response to climate and its variation over time, instead of applying the model from eq. (6) over the whole time series, we applied a sliding window over the NDVI time series to allow a more flexible estimation of the model's parameters.

To remove seasonality effects and to have a long enough time series to estimate the state variable and the parameters with an adequate level of uncertainty, we chose a two-year time window which contained 46 data points. The window was slid from the beginning of the time series on February 18, 2000, to the last data used in the analysis on August 14, 2022, resulting in a total of 495 data points with 449 two-year windows.

2.4.2. Parameter estimation

Once the windows have been defined, we estimated the model parameters by employing the particle filter Sequential Monte Carlo Estimation method (SME), via the use of a sliding window over the observed NDVI time series. In the first step, the model parameters and the corresponding state variables for the first 46 measurements were calculated using a Markov Chain Monte Carlo Method with uninformative a priori distributions to estimate the a posteriori distributions. Starting with the second window, it was applied sequentially on a series of observations, so the parameters a posteriori distribution estimated on a given window were used as a priori distributions for the next window that was offset to the first one by only one data point (or 16 days), therefore they overlap with the next one in 45 of the 46 data points of their length. Then, the distributions were updated and a posteriori distribution results were used for the following window. That procedure was repeated iteratively across the time series As a result, on each step, a series of values drawn from the parameters distribution and state variables from the previous step was used to compute the evolution of the dynamical system until the end of the window of that step.

Each combination of state variables and parameters was named a *particle*. The difference between the estimated and observed values on each window was calculated using a normal log-likelihood function and it was used to give each particle a weight. Then, the best-fitting particles received a higher weight than the others. The particles with lower weights were discarded, and the ones with higher weights were *reproduced* using a random distribution around their estimated value, in a similar way as in a *genetic algorithm* (Kwok et al., 2005).

2.4.3. A priori distributions

The analyzed variables on the model were the logistic regression parameters between K and climatic variables (according to eq. 2), the Gamma distribution parameters (eq. 4), and the growth rate (r), the state variable (the estimated NDVI value) and the linear correlation (r^2) for each NDVI measurement.

For temperatures, the parameters were T_o and T_{sl} which are the

origin and the slope of the linear function being logistically transformed, respectively, to obtain K_t according to eq. 2. For radiation, the same parameters used to calculate K_R were named R_o and R_{sl}. Finally, for rainfall, the parameters were W_o, W_{sl}, α and θ being the origin, slope from the logistic function, shape and scale from the gamma function, respectively.

For all the origin parameters, a Normal a priori distribution was used with an initial mean of -9.2, so when the climatic variable was zero, the estimated K was 0.0001, a value small enough to be indistinguishable from zero (to obtain a real zero, an origin equal to minus infinite is necessary), with a very wide standard deviation (5) so the distribution can be considered uninformative. Normal priors with zero mean, with a standard deviation of 1, were used for the slope, but it was restricted to the range between -2 and 2 to avoid unfeasible local minimums. For α and θ, we used exponential prior distributions with a mean of 1 and 50, respectively, resulting in an average initial Gamma distribution with a mean of 50, mode 0 and a standard deviation of 50 for both variables. The very wide initial values for the Gamma distribution were chosen to account for the different study cases, some of which were wetlands, other grasslands, and other shrub steppes (Table 1). Hence, the response times to rainfall might be highly variable, since they can vary from a few days to several months.

2.4.4. Calculations

The SME procedure was applied on two-year-width sliding windows to remove any seasonal effect. The parameters and state variables fitted to one window were used as input for the next window period. For the first window (i.e. February 2000 to February 2002), since we did not have any previous information, we generated 131,072 random combinations of parameters and kept the best fitting of 256 combinations as the starting particles for the algorithm. Then, the algorithm further improved the fitting by generating 1024 random combinations of parameters based on the selected ones and, again, we kept the best fitting of 256 particles.

Then, from the second window onwards, the algorithm generated 1024 new particles based on the previous 256, distributed according to the relative likelihood between the best-fitting particle and each of the following particles. Again, from these 256 particles and the newly generated 1024 ones, the best 256 fittings were kept for the next iteration. We have chosen that number of particles because, during preliminary runs, they were small enough to avoid overfitting while allowing the parameters to vary and adapt to new conditions. The acceptance ratio of 1/4 was chosen because it is considered a standard metric and it is recommended in the classical Montecarlo methods' literature for drawing a posteriori distributions using rejection sampling (Gelman et al., 2004).

For each iteration, a linear correlation (r^2) between the NDVI estimated by each particle and the observed NDVI over the two-year period window was calculated. The following criterion was defined for this procedure. If none of the particles of the set had an r^2 of at least a zero value (i.e., the fit was worse than a null model), the algorithm kept generating particles until at least one of them had an r^2 of zero or higher.

2.4.5. Analysis of the a posteriori time-series distributions

The resulting output of the model consisted of a matrix of estimated parameters for each time window. The matrix was used to obtain the time series of the parameters a posteriori estimations. These were the intercept and the slope of the linear-logistic function (eq. 2) for each climate variable, plus the parameters of the Gamma function used to convolve the rainfall data (eq. 3), the state variable, and the linear correlation. The mean estimates and the 95% credibility intervals for each of these variables were calculated using 50%, 2.5% and 97.5% quantiles of the estimations on each NDVI measurement date, respectively.

The two parameters used for describing the Gamma function α (shape) and (scale) were converted into mean and standard deviation in

order to make it more easily interpretable, with the mean equal to αθ, and the standard deviation equal to $\sqrt{\alpha\theta^2}$. Those two moments were also called the mean *delay* and *spread* of the convolved time series of the water availability with respect to the rainfall. It should be noticed that delay refers to the *mean* of the distribution and not to the *mode,* which is the moment in time in which the peak of the water availability is reached after the rainfall.

3. Results

3.1. The overall pattern and fitting

The algorithm applied to the pixels time series showed a good fitting with most of the NDVI data from the time series within the 95% credibility interval of the model regression (Fig. 3). The algorithm fitted similarly both in highly seasonal time series (Fig. 3.2 and 3.5) and in series with a less defined seasonality (Fig. 3.1 and 3.6). However, it had trouble with very strong non-seasonal or irregular perturbations, such as in the case of the 2011 depression caused by the volcanic ashfall event, registered in archetype 6 (Fig. 3.6). In addition, irregular *bumps* appeared in some cases, such as archetype 4 in 2019 and 2020 (Fig. 3.4). Overall, these were unpredictable strong departures from the mean.

3.2. Coefficient of determination: a proxy of vegetation response to climate

The model was capable of showing a variation in the explained data variance along the complete studied period. The r^2—as a function of time—showed great variations. For instance, some archetypes evolved from a very high level of fitting to a near-zero level in the span of a few years, and in some cases, they returned to high levels of r^2 again (Fig. 4). In particular, archetype 1 evolved from a moderate-low level of fitting in 2000–2002 to near zero in 2002–2004, and it abruptly increased again to a high level of r^2 close to 0.4 in 2003.5–2005.5 until 2006.5–2008.5, then it decreased again to near zero. That variation was repeated again two more times, settling on near-zero values at the end of the study time window (Fig. 4.1). Archetype 2 started with a high level of r^2 (above 0.6), reached a peak over 0.8 after the window 2005–2007, and began a slow decline to values below 0.2 after 2012–2014, increasing in 2016–2018 but returning to low values in 2018–2020 (Fig. 4.2). For Archetype 3, the r^2 was high with values between 0.4 and 0.6, until 2003–2005 and 2005–2007 when it decayed to near-zero values and increased again to values above 0.6, then it behaved irregularly until 2008–2010 where it decreased and remained in very low values until 2012–2014. After that, r^2 began to increase again and between 2015 and 2016 it reached the same levels as in 2000. Then, it decayed again to near zero and finally increased to above 0.8 at the end of the observation window (Fig. 4.3). Archetype 4 was irregular, showing high-frequency variation in r^2 from near zero to higher values, up to 0.8 along the entire study period (Fig. 4.4). Archetype 5 showed stable and high r^2 values between 0.4 and 0.8, without registering falls to near zero (Fig. 4.5). Finally, archetype 6 was stable at low levels of r^2 until 2009–2011 when it began an upward trend to reach values above 0.4, decaying to near zero again in 2018–2020 (Fig. 4.6).

3.3. Variation of parameters

With respect to the model parameters, they showed important variations among archetypal cases and across time. The slope parameter was a sensitive indicator in registering the behaviour of the different climatic variables used in this study.

All the parameters showed noticeable variations with time (Figs. 4-8). In most of the cases, the variations had the shape of a smooth long-term trend, with few variations from one time window to the next one, being higher than the previous credibility interval. Most of these sharp transitions were present in the parameters related to the Gamma

windows' function used to convolve the rainfall time series in the less seasonal archetypes (i.e. archetypes 1,3,4,6). As the major fluctuations were in the water-availability term of the model in some archetypes, but few as compared to the total number of windows (449), we assume that these variations corresponded mostly to changes in the vegetation dynamics and were not an artefact of overfitting the model's parameters.

3.3.1. Temperature - NDVI slope

Archetypes 1 to 4 showed stable values of the Temperature-K slope. The highest levels were recorded for archetypes 2 and 4 (i.e. highly sensitive to temperature), and the lowest level for archetype 3 (i.e. a marginal sensitivity to temperature). On the other hand, archetypes 5 and 6 showed a slight trend, recording a steady increase of one order of magnitude and a slowly constant decrease, which means an increasing and decreasing sensitivity to temperature, respectively (Fig. 5).

3.3.2. Radiation - NDVI slope

Archetypes 6, 4 and 2 recorded an almost constant trend during the entire observation window. Archetype 1 increased at the beginning of the studied period and then remained at high values after 2003–2005, whereas archetype 5 decreased slightly until 2011–2013, and then recorded slow oscillations. Finally, archetype 3 decreased constantly from 2000 to 2021, which means a decreasing sensitivity to radiation of almost one order of magnitude (Fig. 6).

3.3.3. Water availability - NDVI slope

Archetypes 3, 4 and 6 recorded a slowly increasing trend until the end of the studied period, suggesting a progressively increasing sensitivity to limitations in water availability, whereas archetype 5 remained stable until 2016–2018 but after the said period it began to decrease (Fig. 7). Archetype 1 decreased slowly until 2004–2006 and remained near 0.1 until 2008–2010, positively recovering again until 2012–2014, and after these years it remained stable at high values. Archetype 2 recorded high stable values until 2008–2010, a moment in which it sharply declined two orders of magnitude until 2011–2013, and after this period it stabilized at low values, suggesting an abrupt shift in the sensitivity to limitations in water availability in the second half of the studied period (Fig. 7).

3.4. Rainfall-water availability convolution function

The two parameters from the Gamma function used to convolve with the rainfall time series to obtain the water availability time series showed similar patterns, revealing that the time delay between rainfall, water availability peak (mean of the distribution), and the dispersal of the time in which the water is available (width of the distribution) were highly correlated (Fig. 8). However, that correlation was not constant. The correlation between width and delay was 0.87 (0.87, 0.88) for archetype 1; 0.79 (0.70, 0.86) for archetype 2; 0.86 (0.50, 0.94) for archetype 3; 0.44 (0.25, 0.55) for archetype 4; 0.90 (0.51, 0.92) for archetype 5; and 0.98 (0.96, 0.99) for archetype 6.

The time series for archetype 1 showed that the delay and width transitioned sharply from several months-long of delay and width after 2003.5–2005.5 to only ten days of delay and one-month width (Fig. 8.1). The transition occurred again in the opposite direction near 2006.5–2008.5, then again near 2014.5–2016.5, and finally near 2017–2019, ending in values near one month of delay and width (Fig. 8.1 and Fig. 9.1).

For archetype 2, the variation occurred continuously without any sharp transition: decreasing from the beginning of the series between 2005 and 2009, in terms of both delay (Fig. 8.2) and width (Fig. 9.2), and slowly increasing again until 2014–2016, remaining constant after those dates.

Archetype 3 showed a combination of some sharp transitions and others slower and more continuous. The delay was constant until 2008–2010, a moment in which it sharply increased from a few months
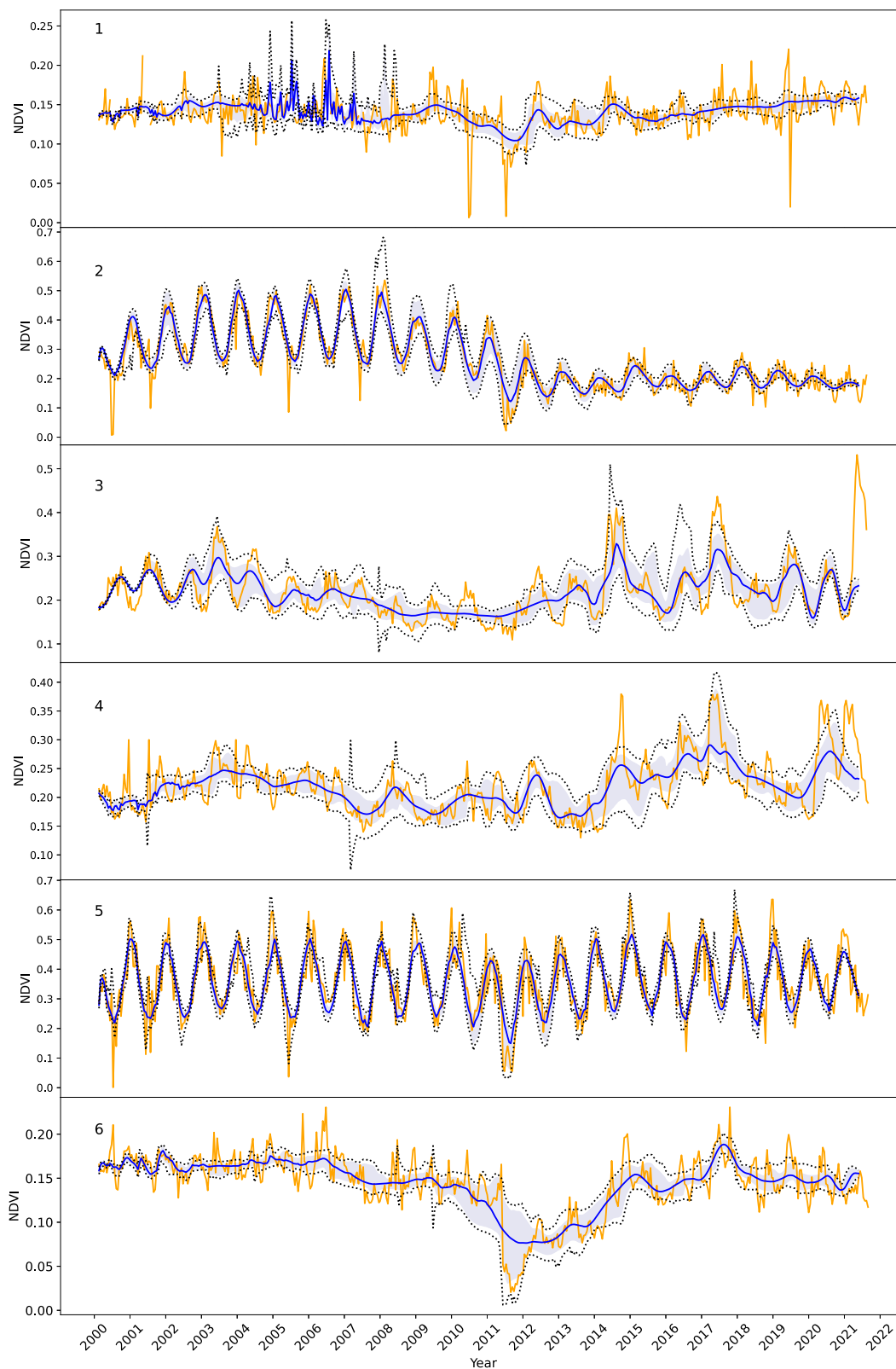
Fig. 3. NDVI time series and model fitted values for the six quasi-archetype pixels used in the study. The order is the same as in Table 1. The continuous blue line is the median estimation, and the light blue area represents 95% of the credibility interval. The dotted lines are the maximum and minimum estimations, whereas the orange lines are the observed time series. (For interpretation of the references to colour in this figure legend, the reader is referred to the web version of this article.)
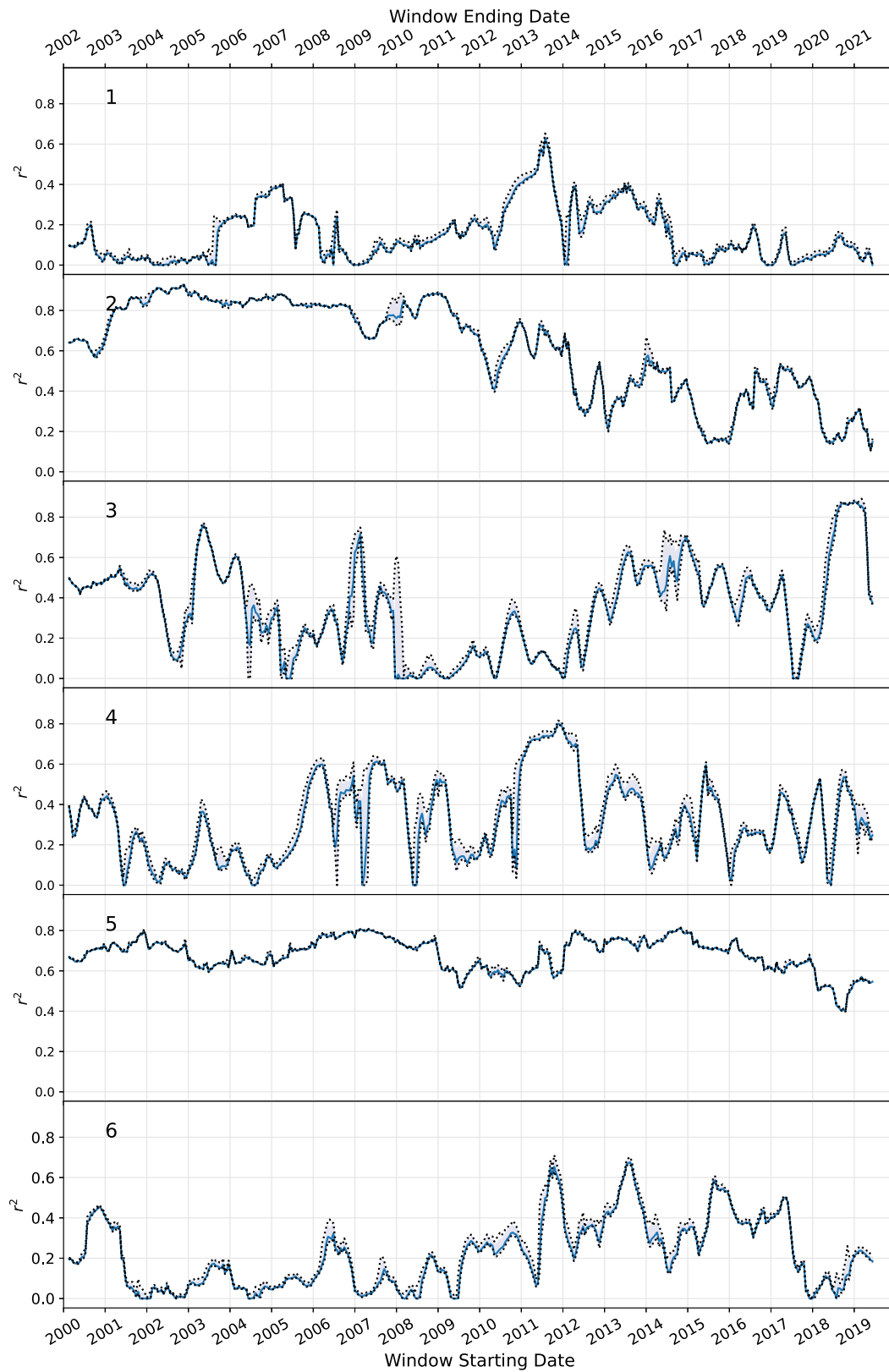
Fig. 4. Determination of linear coefficient (r^2) of the estimated model on each time window for each quasi-archetype pixel. The lower x-axis is the sliding window starting date, and the upper x-axis is that window ending date. The continuous blue line is the median estimation, and the light blue area represents 95% of the credibility interval. The dotted lines are the maximum and minimum estimations. (For interpretation of the references to colour in this figure legend, the reader is referred to the web version of this article.)
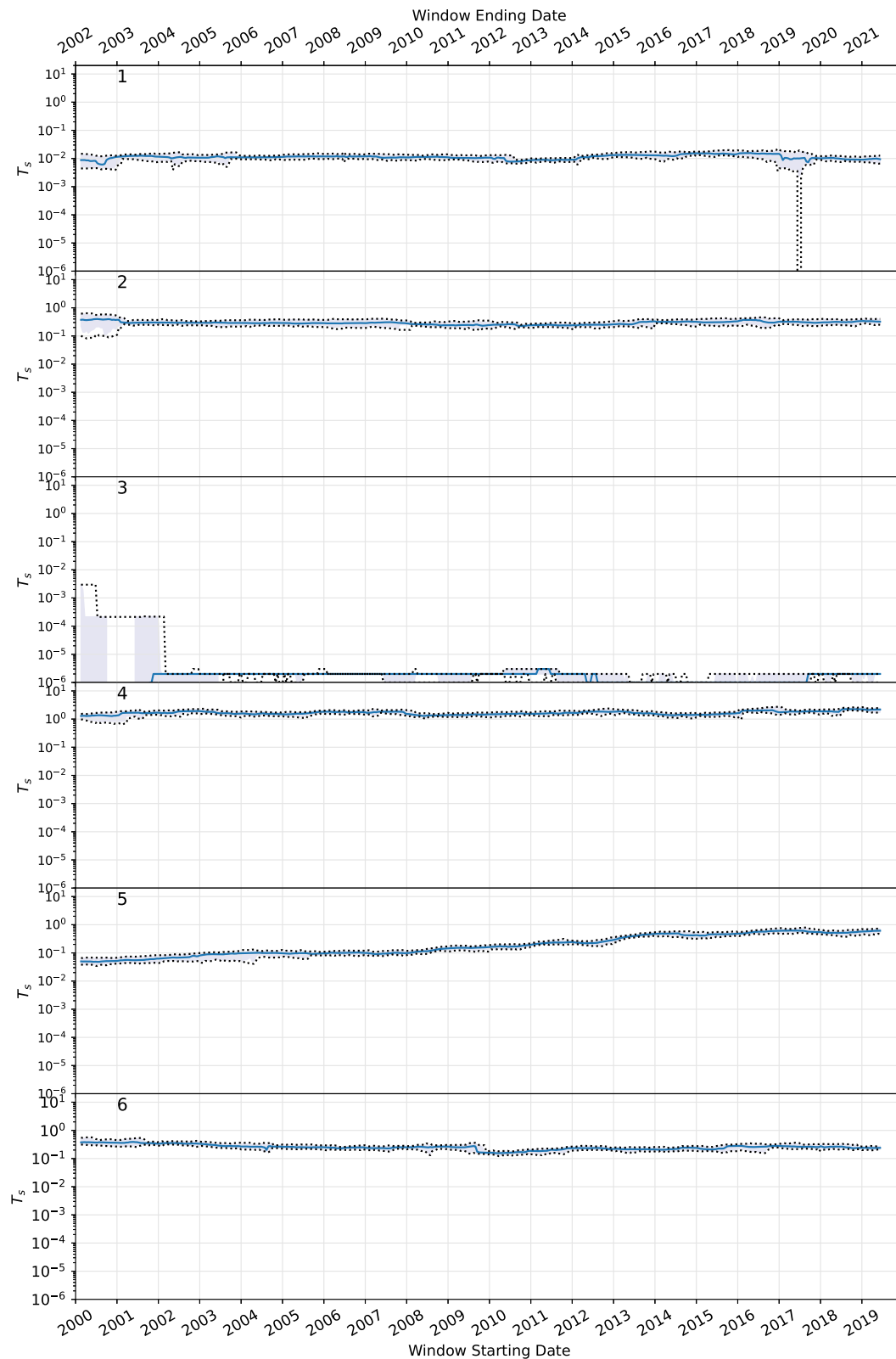
Fig. 5. The slope of the logistic function of K as a function of Temperature (*T*) of the estimated model on each time window for each quasi-archetype pixel. References to the plot are the same as in Fig. 3.

to nearly one year. Then, after 2011–2013, it began to slowly decrease to finally stabilize in values near a month after 2012–2014 (Fig. 8.3). In terms of width, the pattern was similar but with an additional transition from nearly a year to almost two months in 2005.5–2007.5. The

decrease began in 2011–2013 and continued until 2017–2019 when values reached <10 days. Finally, the width began to increase again until stabilizing on values slightly above a month after 2018 (Fig. 9.3).

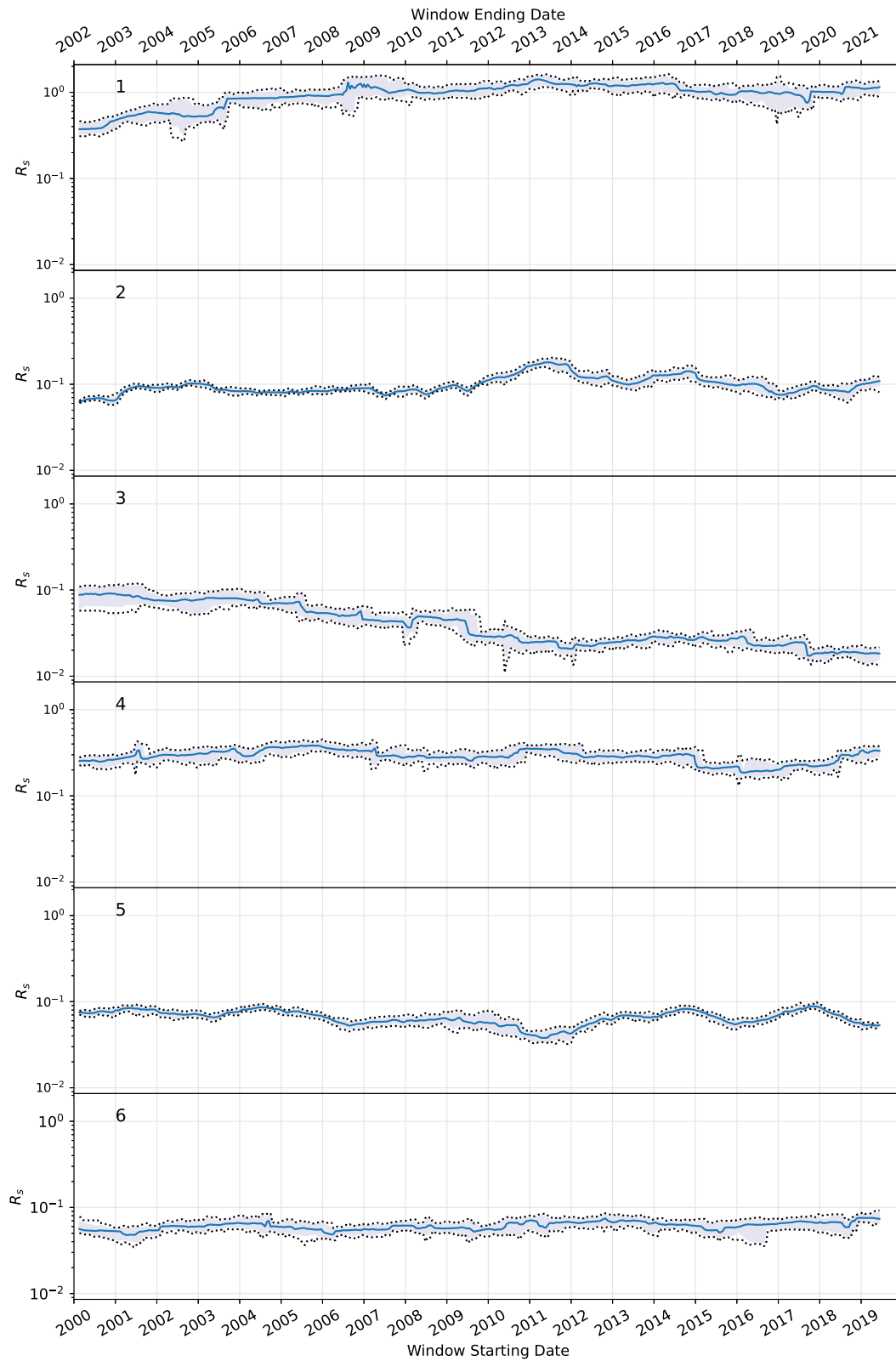Archetype 4 had a fairly stable delay between one and three months

Fig. 6. The slope of the logistic function of K as a function of Radiation (*R*) of the estimated model on each time window for each quasi-archetype pixel. References to the plot are the same as in Fig. 3.

(30 to 100 days) (Fig. 8.4). However, the width varied more strongly between one month to one year several times in the time series, reaching the minimums in 2005–2007, 2016–2018 and 2018.5–2020.5, and the maximums in 2007–2009 and 2009–2011 (Fig. 9.4).

Archetype 5 was stable, averaging near 100 days or three months in the time series for both the delay (Fig. 8.5) and width (Fig. 9.5) variables. Yet, they were the time series with wider credibility intervals most of the time, being several months wide.
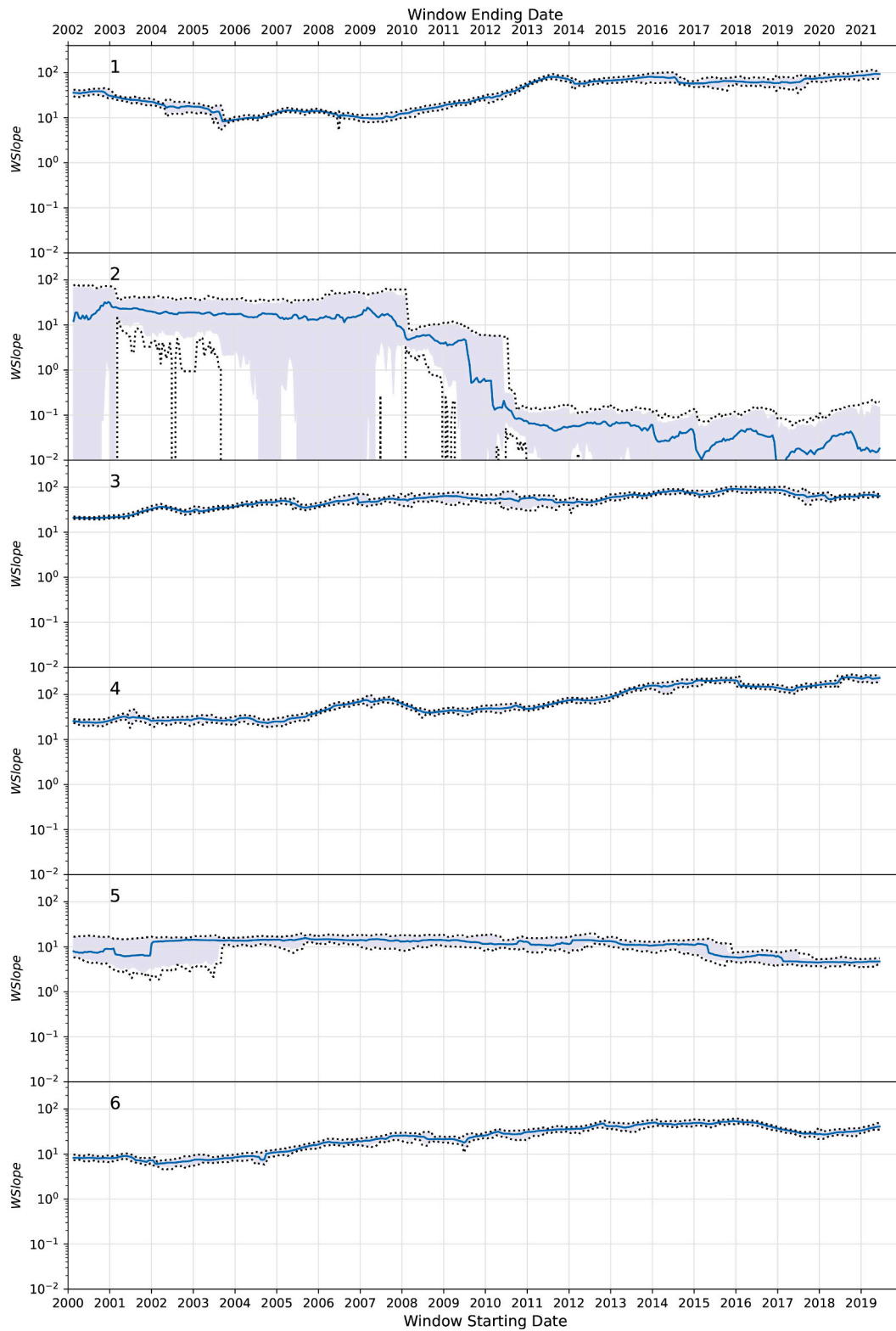
Fig. 7. The slope of the logistic function of K as a function of Water availability (*W*) of the estimated model on each time window for each quasi-archetype pixel. References to the plot are the same as in Fig. 3.

Finally, archetype 7 showed only one strong transition near 2004.5–2006.5, from less than ten days of delay to a month, and from ten days to more than three months (or 100 days). After this period it remained stable, oscillating from one to three months of delays (Fig. 9.6), and from three months to a year of width (Fig. 9.6).

3.5. Growth rate/response time scale

The *r* variable measures the growth rate and, according to this model, it is also the inverse of the time needed to reach *K* at very low levels of NDVI through time. The *r* of archetype 1 decreased several orders of
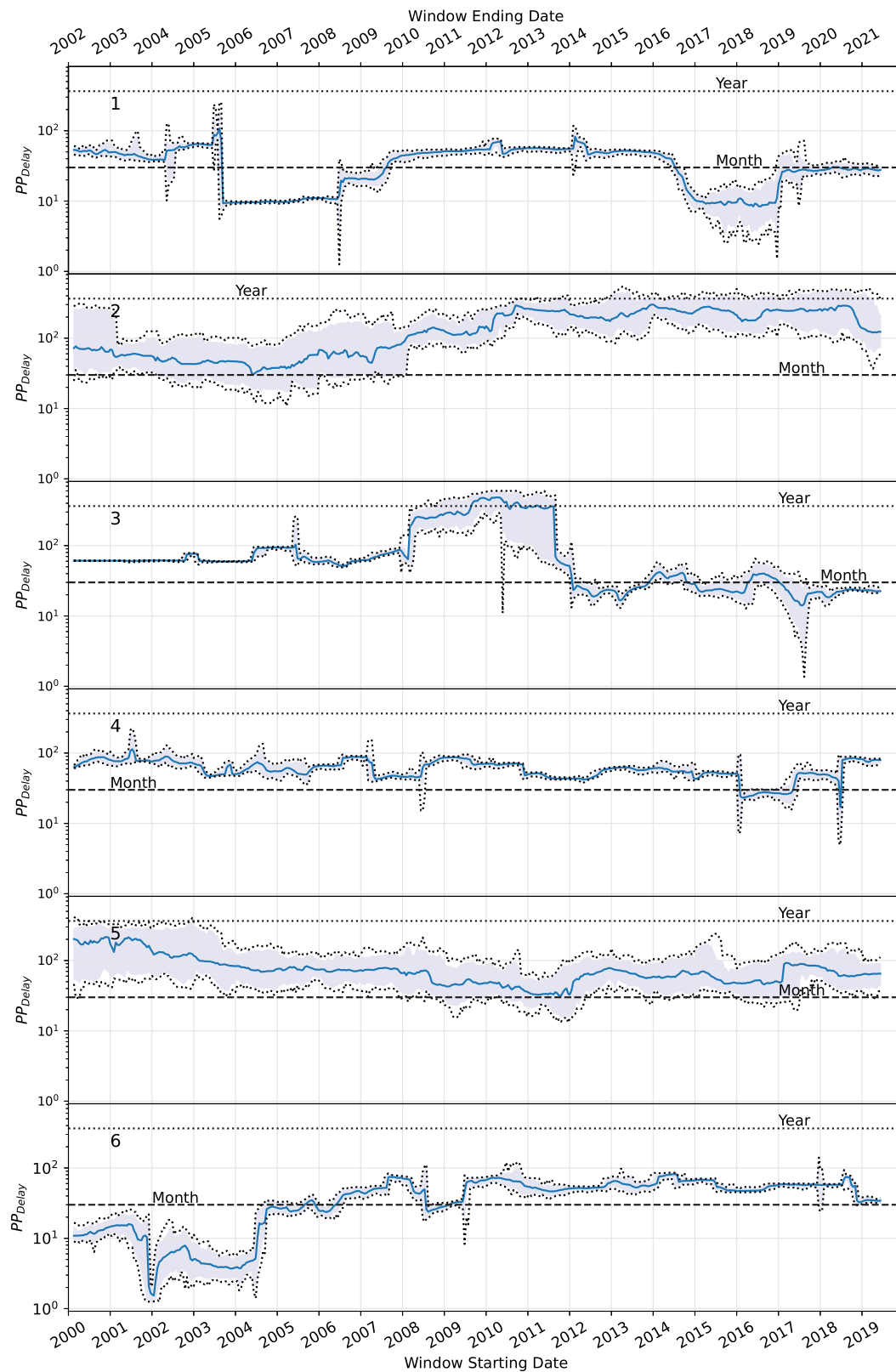
Fig. 8. Response delay to rainfall. Calculated from the gamma distribution function mean, which was utilized to convolve with the rainfall time series to obtain the water availability time series on each time window, for each quasi-archetype pixel. References to the plot are the same as in Fig. 3.

magnitude from the beginning to the end of the studied period. After the 2010.5–2012.5 window it declined to very low levels (below 0.001, Fig. 10), which means that the ecosystem response to climate variations shifted from 10 days to >100 years. In a similar direction, archetypes 2 and 4 recorded a downward trend, meaning that the ecosystem response to climate variations progressively amplified its delay over time. As well, archetype 3 recorded a similar downward pattern from 2000 until 2011–2012, but after that an oscillatory recovery was registered,
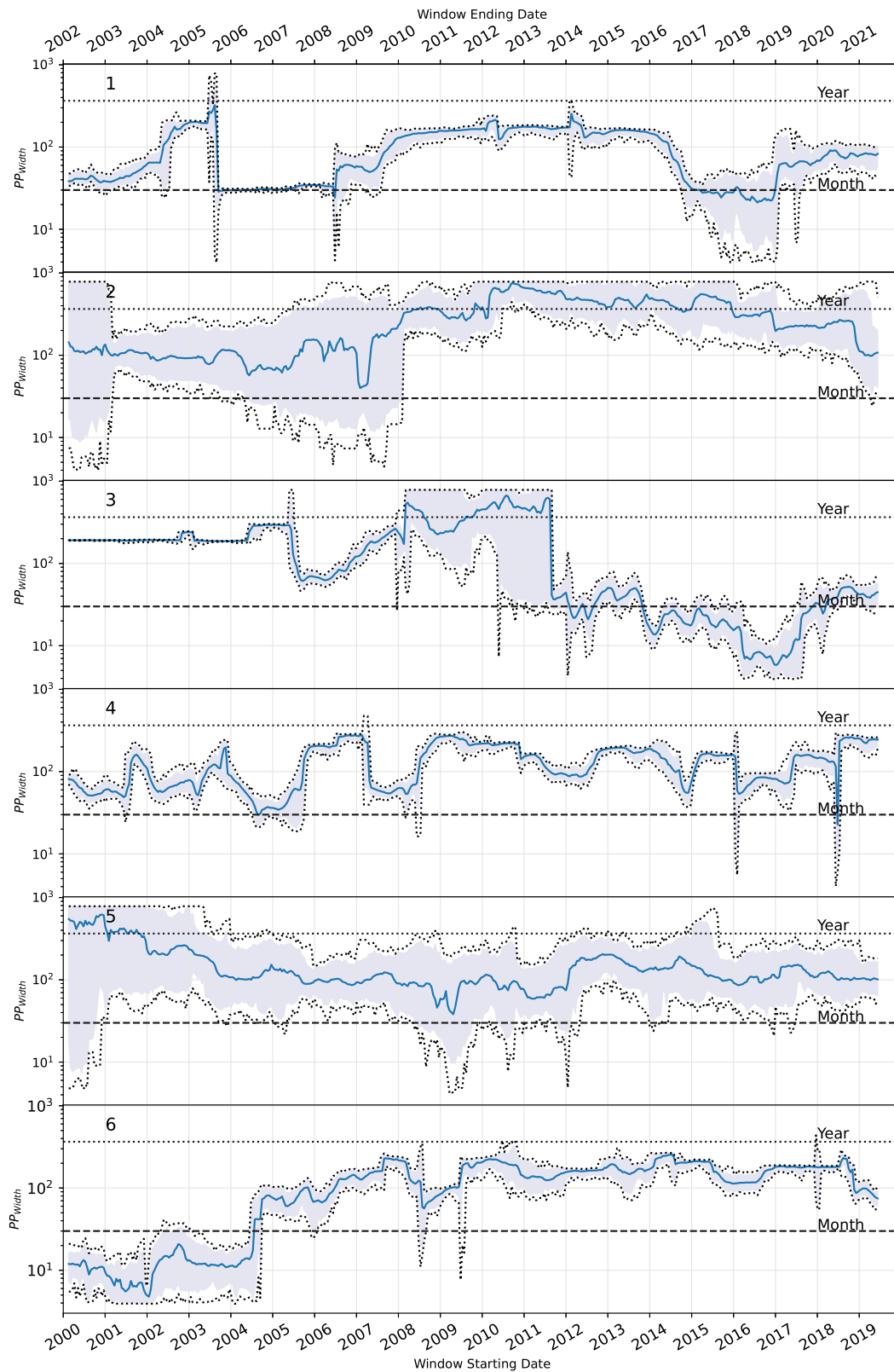
Fig. 9. Integration window *width* in the response to rainfall. Calculated from the standard deviation of the gamma distribution function, which was utilized to convolve with the rainfall time series to obtain the water availability time series on each time window, for each quasi-archetype pixel. References to the plot are the same as in Fig. 3.
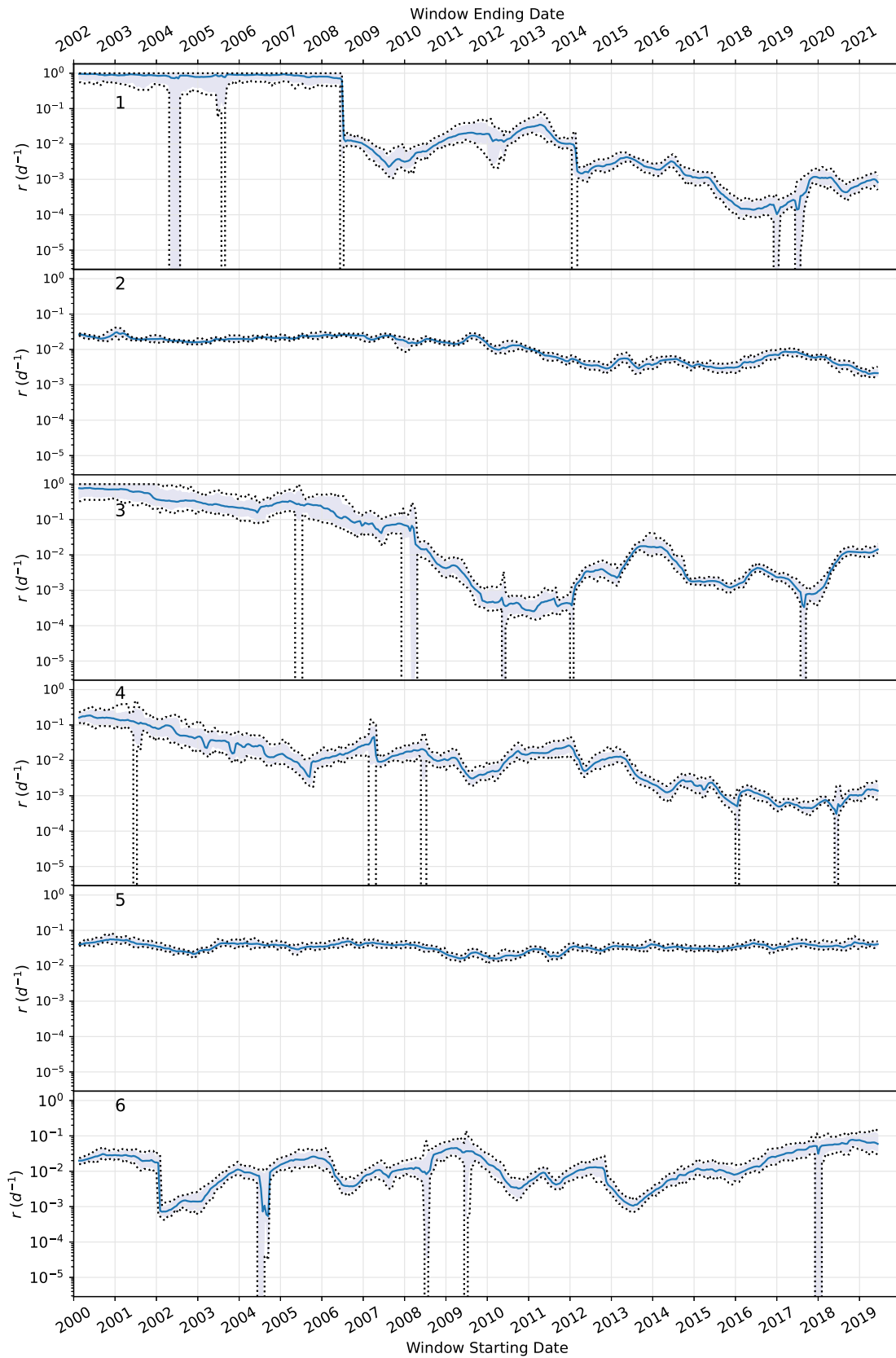
Fig. 10. Growth rate *r* of Brody's growth curve, for each quasi-archetype pixel. References to the plot are the same as in Fig. 3.

reaching an intermediate level. Finally, archetype 5 recorded stable behaviour along the entire studied period, whereas archetype 6 showed an oscillatory upward trend after abrupt shifts at the beginning and at the mid-term of the period (Fig. 10).

4. Discussion

We developed a procedure consisting of a combination between a non-autonomous ODE-based dynamical system and a Sequential Monte Carlo Estimation to study the vegetation temporal response—as measured by the NDVI series 20-year period—to temporal variations in climatic conditions driven by rainfall, temperature and radiation. Very different temporal patterns were recorded in six study cases of rangelands from North Patagonia, Argentina, which suggested sensitiveness in capturing changes in the climate-vegetation system.

The time series analysis based on a posteriori estimated parameters distribution that connects climate with vegetation response allowed further understanding of the causes underlying the ecosystem response capacities under different circumstances. Results showed that most rangelands recorded changes in their sensitivity to climatic factors over the 20 years time frame of the study, but vegetation responses were heterogeneous and influenced by different drivers. For example, climate-vegetation relationships recorded the following patterns: (1) a marginal and decreasing sensitivity to temperature and radiation, respectively (Figs. 5.3 and 6.3), but recorded a high sensitivity to water availability (Fig. 7.3); (2) high and increasing sensitivity to temperature, radiation and water availability, respectively (Fig. 5.4, 6.4 and 7.4); and (3) a case with an abrupt shift in vegetation dynamics (Fig. 3.2) driven by a progressively reducing sensitivity to limitations in water availability (Fig. 7.2), without changes in the sensitivity either to temperature or radiation (Fig. 5.2 and 6.2).

The relevance hierarchy of different climatic and environmental drivers and their impact on vegetation productivity over time can be conceptualised by following Leibig's *Law of the Minimum* (Van der Valk, 2011; Liebig et al., 1842). Under strict and linear conditions of adherence to this law, it might seem that results have a negative correlation between the slopes of the limiting variables, however, it is not the case (Table A1 from the appendix). According to Shelford's *Law of tolerance*, the factors act in concert rather than in isolation, this means that some low levels in one variable might be compensated by higher values of others (Shelford, 1931). If one factor, most likely water availability, is too low for a certain period of time, the plants might start some drought-tolerance mechanism and become inactive (Volaire and Norton, 2006). Low temperatures also cause similar patterns, being the plants dormant during the cold winters with under zero temperatures (Rohde and Bhalerao, 2007). The plant population might become insensitive to all three measured variables by defect and not by excess.

The connectivity between the climate system, ecosystem structure and function has long interested ecological research as it is mediated by a complex behaviour (e.g. Byrne et al., 2017; Foley et al., 1998; Smith et al., 2011). The concept of coupling was defined as the multiple ways in which the biotic and abiotic ecosystem components are orderly connected across space and/or time (Ochoa-Hueso et al., 2021). However, a limitation of these approaches is that coupling is estimated over the complete measurement interval using the same mathematical function. Therefore, the consequences of the advancement of global changes are likely to be underestimated in many conventional analyses, such as stationary-based models, because nonlinear, abrupt and irreversible responses are insufficiently considered (Higgins et al., 2002; Wolkovich et al., 2014). Alternative approaches such as the one presented in this study overcome these limitations, because they self-correct and adjust to new conditions and change the dynamics in terms of the parameters of the studied system.

For instance, the search for breaking points or changes in vegetation dynamics is mostly centred on the analysis of the variation of the average values in the long term such as linear trends (Easdale et al.,

2018). However, sometimes a perturbation might not disrupt the mean but the relationship between the climate-vegetation system, either by slowing down or accelerating the ecosystem response (Ratajczak et al., 2018; Schmitz, 2004) or even by promoting a decoupling of vegetation from the climate via a series of unpredictable random shifts. In this sense, the proposed approach is a promising tool since particle filter methods can self-tune the parameters of the model and measure the changes in the degree and type of climate-ecosystem relationship. Finally, by using this methodology, coupling can be estimated as a probability function, where the shifts in the ecosystem productivity dynamics are mediated over time by shifts in the climatic factors.

Further research is needed to expand the application of our proposed approach in terms of a combination of statistical/regression and dynamic models, with a sequential optimization technique to different regions and biomes. At this stage, the proposed methodology is encouraging as a step forward in building a bridge between the conceptualization of the ecosystem sensitivity to climate change (e.g. Byrne et al., 2017) and the underlying mechanisms of (de)coupling processes between climate drivers and terrestrial ecosystems (Smith et al., 2017).

The local yield of terrestrial plants should be limited by the environmental factor that is present in the environment in the smallest amount relative to its demands for plant growth, which availability changes over time. We acknowledge that more tightly coupled ecosystems displaying higher levels of internal order may be characterised by a more efficient capture, transfer and storage of energy and matter (Ochoa-Hueso et al., 2021), and we understand that the linkages between coupling/decoupling processes and the consequences of changing the climate-ecosystem functioning need further research.

Indeed the approach presented here is a black-box type, so most of the processes underlying the changes in vegetation dynamics are hidden from the analysis, and for a more correct understanding of the processes, field measurements are needed in situ. However, our results are coherent with the findings in previous studies performed in the area or in similar ecosystems from other areas of northern Patagonia (Gaitan et al., 2014). Response to water availability might be related to the partitioning of resource usage (López et al., 2022). It is well documented that Walter's (1971) two-layer hypothesis is supported in the Patagonian ecosystems (Pelaez et al., 1994; Sala et al., 1989). That theory means that grasses take most of the water from the upper layers of soil, whereas shrubs take most of it from the lower layers. As a consequence, grasses and shrubs' response times differ from the rainfall events (Golluscio et al., 1998). The interpretation of this water uptake could be that shrublands respond as a lower-pass filter compared to grasses (Lu et al., 2003), even if the phenological curve is taken into account or if the data are aggregated into an annualized productivity curve. In arid and semiarid ecosystems —characterised by a mixture of shrubs and grasses— the observed response using remotely sensed data has both short-term and long-term information. Under the influence of drought and after some time, the herbaceous vegetation (and all the plants that use the water from the upper layers of soil), might *switch off* from climatic influences, resulting in a wavy-pattern observation mostly driven by woody vegetation (Blanco et al., 2016; Lu et al., 2003). Therefore, the vegetation response to climate might be a stepped function, in which different ecosystem vegetation types respond differently to changes in climatic conditions, ultimately relying on resource availability (i.e. some vegetation turn off their response whereas others keep on responding). Hence, linear functions are not completely adequate to analyze or measure this kind of response (Easdale et al., 2018). However the support for that hypothesis is not uniform, and in areas with non-seasonal rainfall as in Archetypes 1 and 6 (Figs. 2.1, 2.6, 3.1, 3.6), the observed data contradicts that hypothesis (Rodríguez et al., 2007), which will result in an even more complex pattern of on/off switching vegetation dynamics, as shown in the wide variation of the parameter of the Gamma window function (Figs. 8.1, 8.6 and 9.1, 9.6). Thus, the approach using non-autonomous dynamical systems on a sliding

window basis is much more adequate for it, as it allows evaluating when and how these changes may occur.

Other approaches to the dynamics of plant population responses to water availability are based on the *pulse-reserve* hypothesis (Noy-Meir, 1973). It states that a rain event over some value considered *effective* triggers a production response in plants and some of that primary production is used to create reserves. The Ogle and Reynolds (2004) model of the threshold-delay response proposed that after a rainfall above a certain threshold—following some delay in days—the water availability decays exponentially to zero, in the same way as an electrical capacitor. However, these approaches consider that a given plant population is only influenced by local rainfall events, while the availability of water might be dependent on both underground and superficial water movements (i.e. recharge, discharge and flows, depending on topography and geomorphology). These different water movements influence the level of the water table and the available groundwater in general. In the cases of shrubs with deep roots (e.g. cases 3 and 4, Table 1) this is the most important type of water resource. On the other hand, for grasses and other herbaceous plants that live in riparian zones or in wetland ecosystems (e.g. case 5, Table 1), water accumulates mainly by rainfall in a local basin. As shown in Figs. 8 and 9, all the archetypoid pixels experienced changes in the delay and width of the water availability functions. Hence, plant populations in all of these ecosystems responded with mean delays that varied from few days to an entire year. These populations simultaneously varied the time scale of rainfall integration with temporal windows in the same scales as the delay, from a few days to years. Water availability might be further altered by the presence of grazing in the region, sometimes decreasing evapotranspiration (Aguiar et al., 1996; Bisigato and Laphitz, 2009), or increasing it (Pereyra et al., 2017), leading to unpredictable variations as the grazing pressure increases or decreases, since the vegetation structure is as important as climate in the resulting observed dynamics (Gaitan et al., 2014). Then, the proposed approach provides a much better explanation of the dynamics of a system as compared to more classical approaches using the same dataset but does not replace field-based measurements. Further studies in the field, tackling both hydrological and ecophysiological features of the studied rangelands, are necessary to corroborate these findings.

Measuring the degree of interconnection between climate and vegetation dynamics has been approached by means of statistical-based methods such as the Granger causality (e.g. Papagiannopoulou et al., 2017). However, these methods are too dependent on linear relationships and cannot dig directly into the causes of either connection or disconnection, so another set of statistical analyses must be performed to infer the causes of the observed patterns. Other non-parametric and nonlinear methodologies were developed such as the non-parametric Mann-Kendall test and Sen's slope (Luo et al., 2020; Zuo et al., 2021), but share the same shortcomings as the Granger methodology when inferring the causes to explain patterns. The combination of the ODE-based model with a Sequential Monte Carlo Estimation is a procedure that contemplates the complex interactions among different variables, offering a more comprehensive understanding of the overall dynamics. Other approaches that resort to a single variable, without considering interaction with other variables, which might be seen as providing an easier interpretation of dynamic patterns, are too simplistic and therefore misleading in their conclusions. We prevent simplistic explanations, while also avoiding excessively complex models. On one hand, the sliding windows allowed the model to vary its parameters according to some hidden process driven by different factors' dynamics such as soil-water-related vegetation response, as in pulse-reserve or threshold-delay processes, or even plant species replacement. On the other hand, it simplifies the understanding of the vegetation production drivers and the time scales at which it occurs, without dwelling on all the details of the process. The algorithm fitted similarly both in high and less seasonal time series, recording less sensitivity with sudden or irregular perturbations (i.e. non climatic factors such as a volcanic ash fallout event), as

well as irregular *bumps,* which appeared in some cases. An advantage over classical approaches using the complete time series is that the model can be *reset* after a disturbance, and therefore, it can provide a more comprehensive explanation of the dynamics after the event. This capacity is limited, however, by the width of the window and the time resolution of the data. As the windows are slid and overlap each other, the process is smoothed and a very low r^2 might appear in the middle of the transition when the a priori estimated parameters from one window may not be reflective of processes that affect vegetation in the following one. As a result, some incoherent parameter estimations might appear in these stages, such as very high slopes. Hence, caution is advised in the interpretation of the results. Smaller windows might improve this aspect, but they are only possible with higher-frequency data. Nevertheless, at this early stage, results are encouraging for the development of a regional tool aimed at informing ecosystem shifts and transitions in near real-time with high time resolution, which may further serve as a source to promote adaptive and sustainable short-medium term management in the context of climate change.

The fundamental premise that rangelands can exhibit multiple states as a response to internal and external factors is now widely accepted (Bestelmeyer et al., 2017). The State-and-Transition models (STMs) are well-documented conceptual models about how ecosystems respond to disturbances (Westoby et al., 1989). From this perspective, a negative transition towards an undesired state involving a degradation process affecting ecosystem structure and functioning has concentrated particular research interest (López et al., 2011). Whereas ecosystem regime shifts are long-term system reorganizations, they may have profound implications for sustainability (Karunanithi et al., 2008). The identification of environmental drivers of a regime shift is complicated due to the complex interactions (Andersen et al., 2009). For instance, the existence of alternative stable states (or regimes) in climate and ecosystems of vast regions such as the Sahara and Sahel were recorded as the result of strong, nonlinear interactions between vegetation and the atmosphere in a historical timeframe (Foley et al., 2003). However, ecosystems may experience abrupt shifts towards another regime in a period of human observations (Zaldívar et al., 2008) for which the changes become irreversible in the medium term. Our results show that archetype 2 recorded a transition from a highly seasonal and productive ecosystem to low production and noisy dynamics, suggesting a transition towards another state (Fig. 2). A temporary improvement in the climatic conditions by means of a wetter cycle was not enough to recover the previous state dynamics. The model identified that this abrupt shift occurred as a consequence of the ecosystem's loss of sensitivity to water availability (Fig. 6), but not to temperature (Fig. 4).

The approach based on non-autonomous dynamical systems combined with SME provides the quantitative tools needed to move forward with the usage of remote sensing and field data, both integrated under the STM for rangeland management. For instance, it can help in identifying the moment in which the observed transition between states occurs (i.e. in terms of vegetation activity or other remotely sensed variable of the used time series), and to identify the main drivers promoting the shift in terrestrial ecosystems (Fig. 7.2). Up until now, the identification of transitions was mostly performed by time-series breakpoint detection methods (de Jong et al., 2011; Forkel et al., 2013) which are limited to only detecting abrupt variations in the mean (used as a proxy of state). Alternatively, the usage of wavelets provides better opportunities to detect changes in the frequency components of ecological time series (Bruzzone and Easdale, 2021; Easdale and Bruzzone, 2018; Easdale and Bruzzone, 2018; Martínez and Gilabert, 2009), even in the presence of a constant mean. Both approaches, however, still lack the explanatory variables needed to understand the nature of these changes. Our approach attempts to move a step forward in filling the gap in the relationship between climatic measurements and the changes in the vegetation dynamics regime, and its temporal response to climatic drivers.

5. Conclusions

The combination of simple non-autonomous ODE models and Sequential Monte Carlo Estimation was used to develop a model that provides novel information about climate and vegetation dynamics. As compared with other methods, the proposed model provides more detailed information and has a higher temporal resolution on the studied interaction. More importantly, it provides a sound understanding of how vegetation changes over time, as a consequence of shifts in different climate drivers, by means of the time series inspection of the models' parameters a posteriori distribution, in absence of reliable field data, which are needed to parameterize a water balance in the model. Given that the climate-vegetation relationship is more complex than the basic ODE model is able to capture, the use of sliding windows allowed the model to vary its parameters according to some hidden process dynamics (e.g. in relation to soil moisture or different vegetation lags, by

vegetation type or differences in species composition). Consequently, the integrated tool showed sensitivity to capture changes over time in the climate-vegetation relationship system. Indeed, whereas this is a first step towards the development of future models that attempt to better capture the variation of the parameters, its current configuration is a novel source of inspiring hypotheses of the ecosystem response to changes in climatic conditions in different regions worldwide, which needs to be tested and complemented with field data.

Declaration of Competing Interest

None.

Data availability

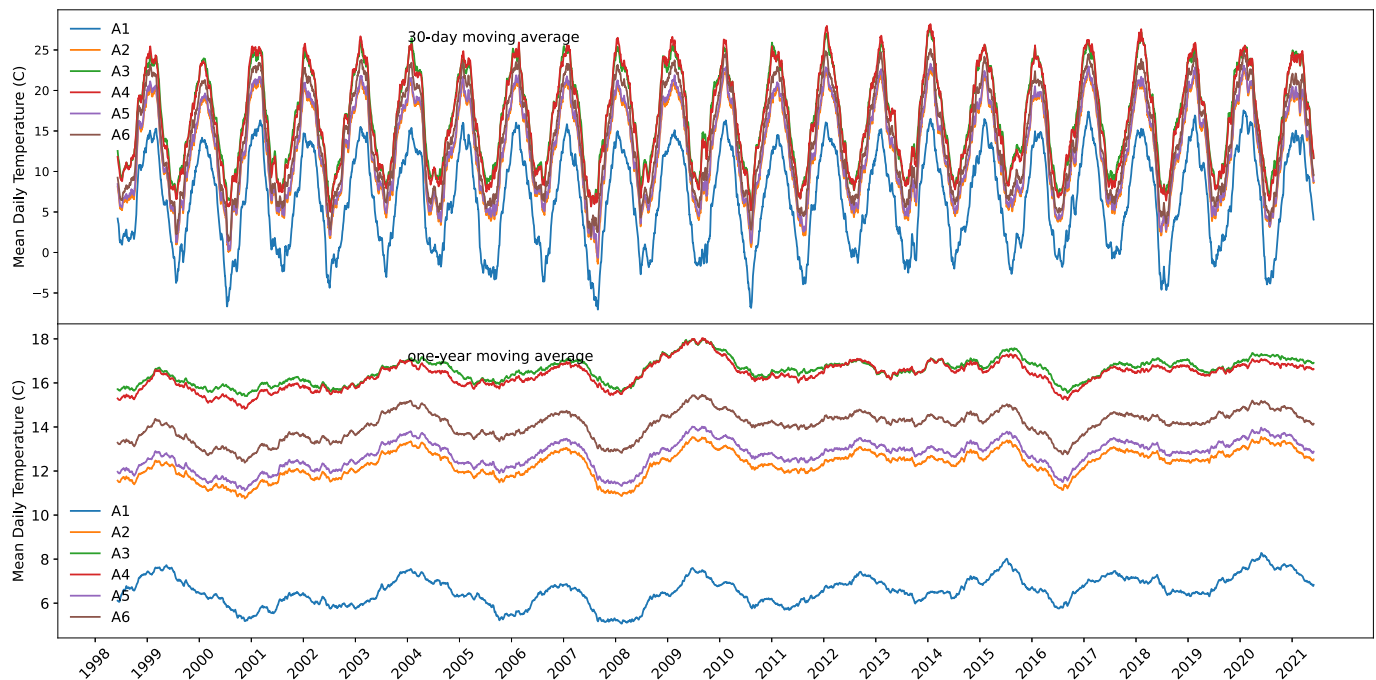Data will be made available on request.

Appendix A. Appendix

Fig. A1 30-days (A) and Annual (B) moving averages of temperature the six studied quasi-archetype pixels. Source of data: ERA5 reanalysis data set (Herbach et al., 2020).
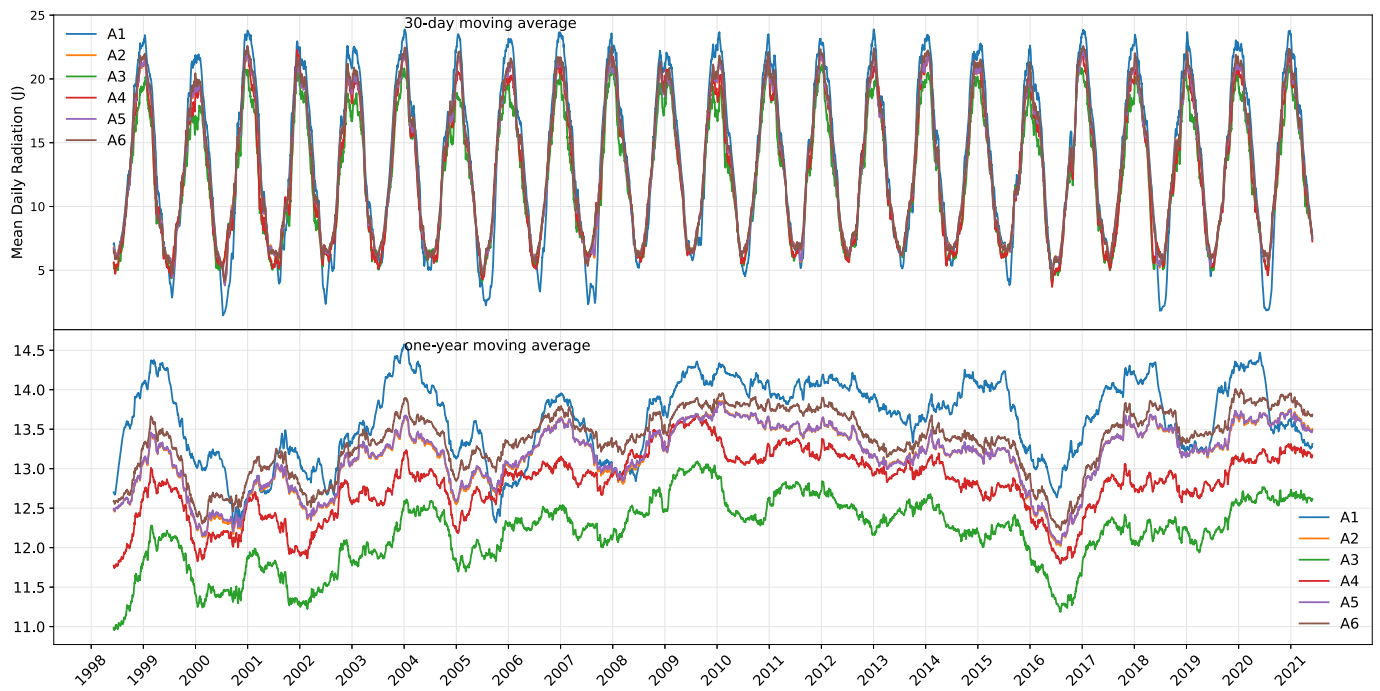
Fig. A2 30-days (A) and Annual (B) moving averages of radiation the six studied quasi-archetype pixels. Source of data: ERA5 reanalysis data set (Herbach et al., 2020).
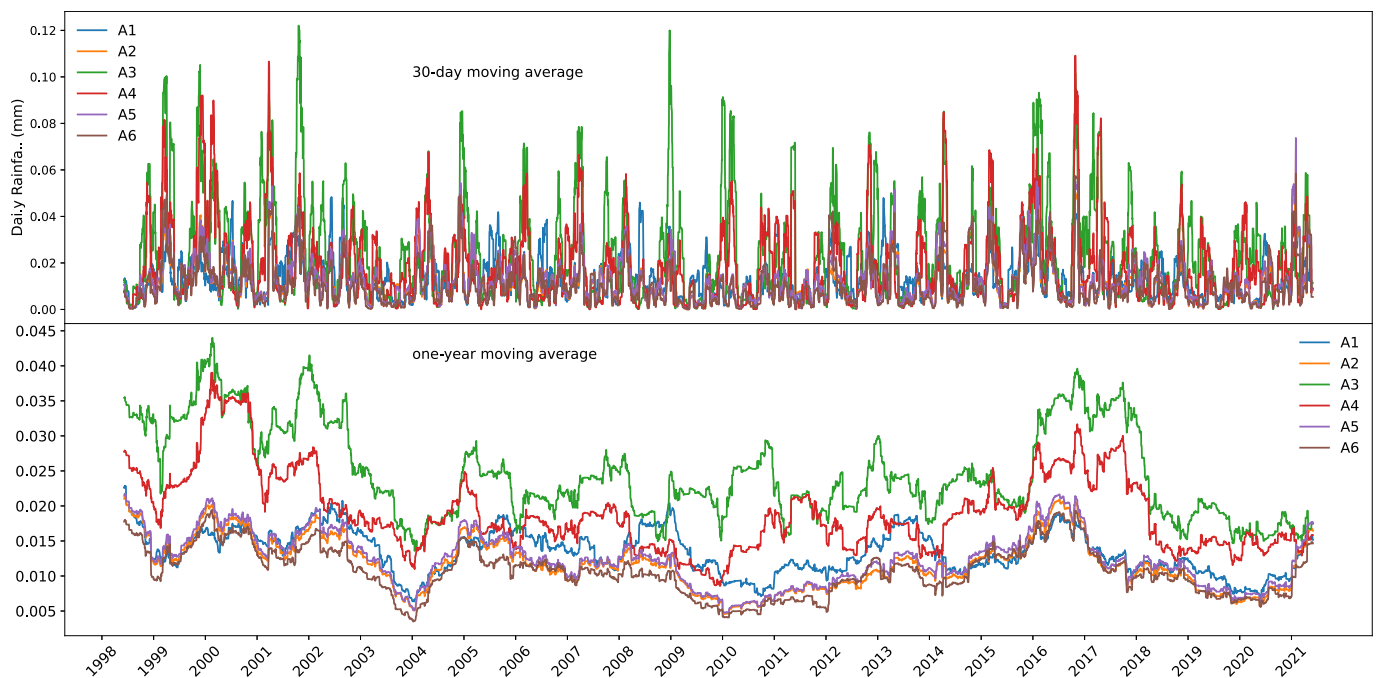

Fig. A3 30-days (A) and Annual (B) moving averages of rainfall the six studied quasi-archetype pixels. Source of data: ERA5 reanalysis data set (Herbach et al., 2020).

Table A1: Correlation table for variables of all the archetypoids, rows in bold are the pairs of variables with strictly behave as expected by Liebig's law of the minimum, that is they have a negative correlation in their slope, so when a variable stops being limiting, and therefore their slope decreases, the other began limiting, and so their slope increases.

Variables		Median	CI 95%
Archetypoid 1			
Temperature slope	Radiation Slope	0.0865	−0.0336, 0.3605
Temperature slope	Rainfall Slope	0.0757	0.0568, 0.1541
Temperature slope	r	−0.1347	−0.4473, −0.3015
Radiation Slope	Rainfall Slope	0.4683	0.4017, 0.4924

(continued on next page)

(*continued*)

Variables		Median	CI 95%
Radiation Slope	r	−0.8062	−0.8152, −0.6515
Rainfall Slope	r	−0.5856	−0.5938, −0.5338
Archetypoid 2			
Temperature slope	**Radiation Slope**	**−0.4383**	**−0.5224, −0.0244**
Temperature slope	Rainfall Slope	0.2344	0.1867, 0.4452
Temperature slope	r	−0.0200	−0.3132, 0.1746
Radiation Slope	**Rainfall Slope**	**−0.5367**	**−0.6220, −0.1415**
Radiation Slope	r	−0.5467	−0.6152, −0.4482
Rainfall Slope	r	0.8381	0.3861, 0.8707
Archetypoid 3			
Temperature slope	Radiation Slope	−0.1814	−0.3089, 0.3296
Temperature slope	Rainfall Slope	−0.0075	−0.3281, 0.1923
Temperature slope	r	−0.4650	−0.5569, 0.4349
Radiation Slope	**Rainfall Slope**	**−0.8001**	**−0.8118, −0.6978**
Radiation Slope	r	0.8786	0.8321, 0.9067
Rainfall Slope	r	−0.7841	−0.8192, −0.7070
Archetypoid 4			
Temperature slope	Radiation Slope	−0.0708	−0.1148, 0.0094
Temperature slope	Rainfall Slope	0.4317	0.3888, 0.4461
Temperature slope	r	−0.2912	−0.5237, −0.1610
Radiation Slope	**Rainfall Slope**	**−0.4762**	**−0.5019, −0.4534**
Radiation Slope	r	−0.0204	−0.0279, −0.0048
Rainfall Slope	r	−0.4756	−0.4836, −0.4522
Archetypoid 5			
Temperature slope	Radiation Slope	−0.0120	−0.0256, 0.0116
Temperature slope	**Rainfall Slope**	**−0.6932**	**−0.8746, −0.4019**
Temperature slope	r	−0.0014	−0.0076, 0.0081
Radiation Slope	**Rainfall Slope**	**−0.1720**	**−0.2854, −0.0586**
Radiation Slope	r	0.4190	0.3192, 0.4826
Rainfall Slope	r	−0.2782	−0.2920, −0.1967
Archetypoid 6			
Temperature slope	**Radiation Slope**	**−0.3613**	**−0.4182, −0.0951**
Temperature slope	**Rainfall Slope**	**−0.5819**	**−0.5943, −0.5732**
Temperature slope	r	0.1299	0.1144, 0.1745
Radiation Slope	Rainfall Slope	0.4359	0.2330, 0.4732
Radiation Slope	r	0.1402	0.0431, 0.2029
Rainfall Slope	r	−0.0094	−0.0115, 0.0036

References

Aguiar, M.R., Paruelo, J.M., Sala, O.E., Lauenroth, W.K., 1996. Ecosystem responses to changes in plant functional type composition: an example from the Patagonian steppe. J. Veg. Sci. 7 (3), 381–390.

Andersen, T., Carstensen, J., Hernandez-Garcia, E., Duarte, C.M., 2009. Ecological thresholds and regime shifts: approaches to identification. Trends Ecol. Evol. 24 (1), 49–57.

Arnell, N.W., Lloyd-Hughes, B., 2014. The global-scale impacts of climate change on water resources and flooding under new climate and socio-economic scenarios. Clim. Chang. 122 (1), 127–140.

Bain, L.J., Engelhardt, M., 1992. Introduction to Probability and Mathematical Statistics. Duxbury Press, Belmont, CA.

Baranyi, J., Roberts, T.A., McClure, P., 1993a. Some properties of a nonautonomous deterministic growth model describing the adjustment of the bacterial population to a new environment. Math. Med. Biol.: A J. IMA 10 (4), 293–299.

Baranyi, J., Roberts, T.A., McClure, P., 1993b. A non-autonomous differential equation to model bacterial growth. Food Microbiol. 10 (1), 43–59.

Besbes, M., De Marsily, G., 1984. From infiltration to recharge: use of a parametric transfer function. J. Hydrol. 74 (3–4), 271–293.

Bestelmeyer, B.T., Ash, A., Brown, J.R., Densambuu, B., Fernández-Giménez, M., Johanson, J., Levi, M., Lopez, D., Peinetti, R., Rumpff, L., Shaver, P., 2017. State and transition models: Theory, applications, and challenges. In: Rangeland Systems. Springer, Cham, pp. 303–345.

Bisigato, A.J., Laphitz, R.M.L., 2009. Ecohydrological effects of grazing-induced degradation in the Patagonian Monte, Argentina. Austral Ecol. 34 (5), 545–557.

Bisigato, A.J., Hardtke, L., del Valle, H.F., 2013. Soil as a capacitor: considering soil water content improves temporal models of productivity. J. Arid Environ. 98, 88–92.

Blanco, L.J., Paruelo, J.M., Oesterheld, M., Biurrun, F.N., 2016. Spatial and temporal patterns of herbaceous primary production in semi-arid shrublands: a remote sensing approach. J. Veg. Sci. 27 (4), 716–727.

Briere, J.F., Pracros, P., Le Roux, A.Y., Pierre, J.S., 1999. A novel rate model of temperature-dependent development for arthropods. Environ. Entomol. 28 (1), 22–29.

Bruzzone, O., Easdale, M.H., 2021. Archetypal temporal dynamics of arid and semi-arid rangelands. Remote Sens. Environ. 254, 112279.

Bruzzone, O.A., Utgés, M.E., 2022. Analysis of the invasion of a city by Aedes aegypti via mathematical models and Bayesian statistics. Theor. Ecol. 15 (1), 65–80.

Byrne, K.M., Adler, P.B., Lauenroth, W.K., 2017. Contrasting effects of precipitation manipulations in two Great Plains plant communities. J. Veg. Sci. 28 (2), 238–249.

Çamdevýren, H., Demýr, N., Kanik, A., Keskýn, S., 2005. Use of principal component scores in multiple linear regression models for prediction of chlorophyll-a in reservoirs. Ecol. Model. 181 (4), 581–589.

Chakraborty, S., Banerjee, A., Gupta, S., Papandreou-Suppappola, A., Christensen, P., 2017. Estimation of dynamic parameters of MODIS NDVI time series nonlinear model using particle filtering. In: 2017 IEEE International Geoscience and Remote Sensing Symposium (IGARSS). IEEE, pp. 1091–1094.

Claeskens, G., Hjort, N.L., 2008. Model Selection and Model Averaging. Cambridge Books.

Coleman, B.D., 1979. Nonautonomous logistic equations as models of the adjustment of populations to environmental change. Math. Biosci. 45 (3–4), 159–173.

Collenteur, Bakker, Caljé, Klop, Schaars, 2019. Pastas: open source software for the analysis of groundwater time series. Groundwater 57 (6), 877–885.

Cook, B.I., Mankin, J.S., Anchukaitis, K.J., 2018. Climate change and drought: from past to future. Curr. Clim. Change Reports 4 (2), 164–179.

Crosbie, R.S., Binning, P., Kalma, J.D., 2005. A time series approach to inferring groundwater recharge using the water table fluctuation method. Water Resour. Res. 41 (1).

De Bernardis, C., Vicente-Guijalba, F., Martinez-Marin, T., Lopez-Sanchez, J.M., 2016a. Particle filter approach for real-time estimation of crop phenological states using time series of NDVI images. Remote Sens. 8 (7), 610.

De Bernardis, C., Vicente-Guijalba, F., Martinez-Marin, T., Lopez-Sanchez, J.M., 2016b. Contribution to real-time estimation of crop phenological states in a dynamical framework based on NDVI time series: data fusion with SAR and temperature. IEEE J. Selec. Top. Appl. Earth Observ. Remote Sens. 9 (8), 3512–3523.

Del Moral, Pierre, 1996. Non linear filtering: interacting particle solution. Markov Proc. Rel. Fields. 2 (4), 555–580.

Díaz-Villa, Bruzzone, Goldstein, Cristiano, 2022. Climatic determinants of photosynthetic activity in humid subtropical forests under different forestry activities. Remote Sens. Appl.: Soc. Environ. 26, 100735 https://doi.org/10.1016/j.rsase.2022.100735.

Diks, C., Wolski, M., 2016. Nonlinear granger causality: guidelines for multivariate analysis. J. Appl. Econ. 31 (7), 1333–1351.

Easdale, M.H., Bruzzone, O., 2018. Spatial distribution of volcanic ash deposits of 2011 Puyehue-Cordón Caulle eruption in Patagonia as measured by a perturbation in NDVI temporal dynamics. J. Volcanol. Geotherm. Res. 353, 11–17.

Easdale, M.H., Aguiar, M.R., Román, M., Villagra, S.E., 2009. Comparación socio-económica de dos regiones biofísicas: los sistemas ganaderos de Río Negro, Argentina. Cuadernos de Desarrollo Rural 62, 173–198.

Easdale, M.H., Bruzzone, O., Mapfumo, P., Tittonell, P., 2018. Phases or regimes? Revisiting NDVI trends as proxies for land degradation. Land Degrad. Dev. 29, 433–445.

Easdale, M.H., Perri, D., Bruzzone, O.A., 2022. Arid and semiarid rangeland responses to non-stationary temporal dynamics of environmental drivers. Remote Sens. Appl.: Soc. Environ. 27, 100796.

Foley, J.A., Levis, S., Prentice, I.C., Pollard, D., Thompson, S.L., 1998. Coupling dynamic models of climate and vegetation. Glob. Chang. Biol. 4 (5), 561–579.

Foley, J.A., Coe, M.T., Scheffer, M., Wang, G., 2003. Regime shifts in the Sahara and Sahel: interactions between ecological and climatic systems in northern Africa. Ecosystems 6 (6), 524–532.

Forkel, M., Carvalhais, N., Verbesselt, J., Mahecha, M.D., Neigh, C.S., Reichstein, M., 2013. Trend change detection in NDVI time series: effects of inter-annual variability and methodology. Remote Sens. 5 (5), 2113–2144.

Friston, K., Moran, R., Seth, A.K., 2013. Analysing connectivity with Granger causality and dynamic causal modelling. Curr. Opin. Neurobiol. 23 (2), 172–178.

Gaitan, J.J., Oliva, G.E., Bran, D.E., Maestre, F.T., Aguiar, M.R., Jobbagy, E.G., Buono, G.G., Ferrante, D., Nakamatsu, V.B., Ciari, G., Salomone, J.M., 2014. Vegetation structure is as important as climate for explaining ecosystem function across Patagonian rangelands. J. Ecol. 102 (6), 1419–1428.

Gelman, A., Carlin, J.B., Stern, H.S., Rubin, D.B., 2004. Bayesian Data Analysis Chapman & Hall. CRC Texts in Statistical Science.

Godagnone, R.E., Bran, D. (Eds.), 2009. Inventario integrado de los recursos naturales de la provincia de Río Negro: geología, hidrología, geomorfología, suelos, clima, vegetación y fauna. Ediciones INTA, p. 391.

Golluscio, R.A., Sala, O.E., Lauenroth, W.K., 1998. Differential use of large summer rainfall events by shrubs and grasses: a manipulative experiment in the Patagonian steppe. Oecologia 115 (1), 17–25.

Granger, C.W., 1969. Investigating causal relations by econometric models and cross-spectral methods. Economet.: J. Economet. Soc. 424–438.

Hallam, T.G., Clark, C.E., 1981. Non-autonomous logistic equations as models of populations in a deteriorating environment. J. Theor. Biol. 93 (2), 303–311.

Hedengren, J.D., Shishavan, R.A., Powell, K.M., Edgar, T.F., 2014. Nonlinear modeling, estimation and predictive control in APMonitor. Comput. Chem. Eng. 70, 133–148.

Hersbach, H., Bell, B., Berrisford, P., Hirahara, S., Horányi, A., Muñoz-Sabater, J., Thépaut, J.N., 2020. The ERA5 global reanalysis. Q. J. R. Meteorol. Soc. 146 (730), 1999–2049.

Higgins, P.A., Mastrandrea, M.D., Schneider, S.H., 2002. Dynamics of climate and ecosystem coupling: abrupt changes and multiple equilibria. Philos. Trans. R. Soc. Lond. Ser. B Biol. Sci. 357 (1421), 647–655.

Hooker Jr., H.D., 1917. Liebig's law of the minimum in relation to general biological problems. Science 46 (1183), 197–204.

Hou, W., Gao, J., Wu, S., Dai, E., 2015. Interannual variations in growing-season NDVI and its correlation with climate variables in the southwestern karst region of China. Remote Sens. 7 (9), 11105–11124.

Husak, G.J., Michaelsen, J., Funk, C., 2007. Use of the gamma distribution to represent monthly rainfall in Africa for drought monitoring applications. Intern. J. Climatol.: A J. Roy. Meteorol. Soc. 27 (7), 935–944.

Ikeda, S., Yokoi, T., 1980. Fish population dynamics under nutrient enrichment—a case of the East Seto Inland Sea. Ecol. Model. 10 (3–4), 141–165.

Jehn, F.U., Chamorro, A., Houska, T., Breuer, L., 2019. Trade-offs between parameter constraints and model realism: a case study. Sci. Rep. 9 (1), 1–12.

Jobbágy, E.G., Sala, O.E., Paruelo, J.M., 2002. Patterns and controls of primary production in the Patagonian steppe: a remote sensing approach. Ecology 83 (2), 307–319.

Johnson, I.R., Chapman, D.F., Snow, V.O., Eckard, R.J., Parsons, A.J., Lambert, M.G., Cullen, B.R., 2008. DairyMod and EcoMod: biophysical pasture-simulation models for Australia and New Zealand. Aust. J. Exp. Agric. 48 (5), 621–631.

Jones, J.W., Hoogenboom, G., Porter, C.H., Boote, K.J., Batchelor, W.D., Hunt, L.A., Ritchie, J.T., 2003. The DSSAT cropping system model. Eur. J. Agron. 18 (3–4), 235–265.

de Jong, R., Verbesselt, J., Schaepman, M.E., de Bruin, S., 2011. Detection of breakpoints in global NDVI time series. 34th International Symposium on Remote Sensing of Environment (ISRSE). In: https://www.isprs.org/proceedings/2011/isrse-34/211104015Final00234.pdf.

Kalman, 1960. A New Approach to Linear Filtering and Prediction Problems. J. Basic Eng. 82 (1), 35–45. https://doi.org/10.1115/1.3662552.

Karunanithi, A.T., Cabezas, H., Frieden, B.R., Pawlowski, C.W., 2008. Detection and assessment of ecosystem regime shifts from fisher information. Ecol. Soc. 13 (1).

Kaufmann, R.K., Zhou, L., Myneni, R.B., Tucker, C.J., Slayback, D., Shabanov, N.V., Pinzon, J., 2003. The effect of vegetation on surface temperature: a statistical analysis of NDVI and climate data. Geophys. Res. Lett. 30 (22).

Kleynhans, Olivier, Wessels, Salmon, Van den Bergh, Steenkamp, 2010. Detecting land cover change using an extended Kalman filter on MODIS NDVI time-series data. IEEE Geosci. Remote Sens. Lett. 8 (3), 507–511.

Kogan, Zhu, 2001. Evolution of long-term errors in NDVI time series: 1985–1999. Adv. Space Res. 28 (1), 149–153.

Kwok, N.M., Fang, G., Zhou, W., 2005. Evolutionary particle filter: Re-sampling from the genetic algorithm perspective. In: 2005 IEEE/RSJ International Conference on Intelligent Robots and Systems. IEEE, pp. 2935–2940.

Landau, H.J., 1967. Sampling, data transmission, and the Nyquist rate. Proc. IEEE 55 (10), 1701–1706.

Liebig, J., Von, F., Playfair, L., 1842. Chemistry in its Application to Agriculture and Physiology. http://resource.nlm.nih.gov/101144937.

Logan, J.A., Wollkind, D.J., Hoyt, S.C., Tanigoshi, L.K., 1976. An analytic model for description of temperature dependent rate phenomena in arthropods. Environ. Entomol. 5 (6), 1133–1140.

López, D.R., Cavallero, L., Brizuela, M.A., Aguiar, M.R., 2011. Ecosystemic structural–functional approach of the state and transition model. Appl. Veg. Sci. 14 (1), 6–16.

López, D.R., Cavallero, L., Willems, P., Bestelmeyer, B.T., Brizuela, M.A., 2022. Degradation influences equilibrium and non-equilibrium dynamics in rangelands: implications in resilience and stability. Appl. Veg. Sci. 25 (3), 12670.

Lu, H., Raupach, M., McVicar, T., Barrett, D., 2003. Decomposition of vegetation cover into woody and herbaceous components using AVHRR NDVI time series. Remote Sens. Environ. 86, 1–18.

Luo, N., Mao, D., Wen, B., Liu, X., 2020. Climate change affected vegetation dynamics in the northern Xinjiang of China: evaluation by SPEI and NDVI. Land 9 (3), 90.

Martínez, B., Gilabert, M.A., 2009. Vegetation dynamics from NDVI time series analysis using the wavelet transform. Remote Sens. Environ. 113 (9), 1823–1842.

Martinez-Villalobos, C., Neelin, J.D., 2019. Why do precipitation intensities tend to follow gamma distributions? J. Atmos. Sci. 76 (11), 3611–3631.

McCune, B., 2011. Nonparametric Multiplicative Regression for Habitat Modeling. Oregon State University. http://www.pcord.com/NPMRintro.pdf>.

Menenti, M., Jia, L., Azzali, S., Roerink, G., Gonzalez-Loyarte, M., Leguizamon, S., 2010. Analysis of vegetation response to climate variability using extended time series of multispectral satellite images. In: Maselli, F., Menenti, M., Brivio, P.A (Eds.), Remote Sensing Optical Observations of Vegetation Properties, Chapter 6, pp. 131–163.

Mitchell, W.F., 2015. How high a degree is high enough for high order finite elements? Proc. Comp. Sci. 51, 246–255.

Moore, J.C., 2018. Predicting tipping points in complex environmental systems. Proc. Natl. Acad. Sci. 115 (4), 635–636.

Nakanwagi, M.J., Sseremba, G., Kabod, N.P., Masanza, M., Kizito, E.B., 2020. Identification of growth stage-specific watering thresholds for drought screening in Solanum aethiopicum Shum. Sci. Rep. 10 (1), 1–11.

Noy-Meir, I., 1973. Desert ecosystems: environment and producers. Annu. Rev. Ecol. Syst. 4 (1), 25–51.

Noy-Meir, I., 1975. Stability of Grazing Systems: An Application of Predator-Prey Graphs. J. Ecol. 63 (2), 459–481. https://doi.org/10.2307/2258730.

Ochoa-Hueso, R., Delgado-Baquerizo, M., Risch, A.C., Schrama, M., Morriën, E., Barmentlo, S.H., Geisen, S., Hannula, S.E., Resch, M.C., Snoek, B.L., van der Putten, W.H., 2021. Ecosystem coupling: a unifying framework to understand the functioning and recovery of ecosystems. One Earth 4 (7), 951–966.

Ogle, K., Reynolds, J.F., 2004. Plant responses to precipitation in desert ecosystems: integrating functional types, pulses, thresholds, and delays. Oecologia 141 (2), 282–294.

Oudin, L., Andréassian, V., Perrin, C., Anctil, F., 2004. Locating the sources of low-pass behavior within rainfall-runoff models. Water Resour. Res. 40 (11).

Papagiannopoulou, C., Miralles, D.G., Decubber, S., Demuzere, M., Verhoest, N.E., Dorigo, W.A., Waegeman, W., 2017. A non-linear Granger-causality framework to investigate climate–vegetation dynamics. Geosci. Model Dev. 10 (5), 1945–1960.

Pelaez, D.V., Distel, R.A., Boo, R.M., Elia, O.R., Mayor, M.D., 1994. Water relations between shrubs and grasses in semi-arid Argentina. J. Arid Environ. 27 (1), 71–78.

Pereyra, D.A., Bucci, S.J., Arias, N.S., Ciano, N., Cristiano, P.M., Goldstein, G., Scholz, F.G., 2017. Grazing increases evapotranspiration without the cost of lowering soil water storages in arid ecosystems. Ecohydrology 10 (6), e1850.

Persson, J., Brett, M.T., Vrede, T., Ravet, J.L., 2007. Food quantity and quality regulation of trophic transfer between primary producers and a keystone grazer (Daphnia) in pelagic freshwater food webs. Oikos 116 (7), 1152–1163.

Poff, N.L., 2002. Ecological response to and management of increased flooding caused by climate change. Philos. Trans. R. Soc. London, Ser. A 360 (1796), 1497–1510.

Pokhrel, Y., Felfelani, F., Satoh, Y., Boulange, J., Burek, P., Gädeke, A., Gerten, D., Gosling, S.N., Grillakis, M., Gudmundsson, L., Hanasaki, N., et al., 2021. Global terrestrial water storage and drought severity under climate change. Nat. Clim. Chang. 11 (3), 226–233.

Rao, C.V., Rawlings, J.B., Maynes, D.Q., 2003. Constrained state estimation for nonlinear discrete-time systems: stability and moving horizon approximations. IEEE Trans. Autom. Control 48 (2), 246–258.

Ratajczak, Z., Carpenter, S.R., Ives, A.R., Kucharik, C.J., Ramiadantsoa, T., Stegner, M.A., Williams, J.W., Zhang, J., Turner, M.G., 2018. Abrupt change in ecological systems: inference and diagnosis. Trends Ecol. Evol. 33 (7), 513–526.

Rawlings, James B., 2009. Model Predictive Control: Theory and Design. Mathematics in Science and Engineering. Nob Hill Publishing, LLC, Madison, WI, p. 576.

Rodríguez, M., Bertiller, M.B., Bisigato, A., 2007. Are fine roots of both shrubs and perennial grasses able to occupy the upper soil layer? A case study in the arid Patagonian Monte with non-seasonal precipitation. Plant Soil 300 (1), 281–288.

Roerink, G.J., Menenti, M., Soepboer, W., Su, Z., 2003. Assessment of climate impact on vegetation dynamics by using remote sensing. Phys. Chem. Earth, Parts A/B/C 28 (1–3), 103–109.

Rohde, A., Bhalerao, R.P., 2007. Plant dormancy in the perennial context. Trends Plant Sci. 12 (5), 217–223.

Rosenbaum, B., Rall, B.C., 2018. Fitting functional responses: direct parameter estimation by simulating differential equations. Methods Ecol. Evol. 9 (10), 2076–2090.

Rosenblatt, M., 1956. A central limit theorem and a strong mixing condition. Proc. Natl. Acad. Sci. 42 (1), 43–47.

Sala, O.E., Golluscio, R.A., Lauenroth, W.K., Soriano, A., 1989. Resource partitioning between shrubs and grasses in the Patagonian steppe. Oecologia 81 (4), 501–505.

Sala, O.E., Chapin, F.S., Armesto, J.J., Berlow, E., Bloomfield, J., Dirzo, R., Huber-Sanwald, E., Huenneke, L.F., Jackson, R.B., Kinzig, A., Leemans, R., 2000. Global biodiversity scenarios for the year 2100. Science 287 (5459), 1770–1774.

Samanta, G., 2012. Analysis of nonautonomous two species system in a polluted environment. Math. Slovaca 62 (3), 567–586.

Schmitz, O.J., 2004. Perturbation and abrupt shift in trophic control of biodiversity and productivity. Ecol. Lett. 7 (5), 403–409.

Sedano, Kempeneers, Hurtt, 2014. A Kalman filter-based method to generate continuous time series of medium-resolution NDVI images. Remote Sens. 6 (12), 12381–12408.

Sharov, A., 1996. Quantitative Population Ecology. http://www.ento.vt.edu/~sharov/PopEcol/popecol.html.

Sharpe, P.J., DeMichele, D.W., 1977. Reaction kinetics of poikilotherm development. J. Theor. Biol. 64 (4), 649–670.

Shelford, V.E., 1931. Some concepts of bioecology. Ecology 12 (3), 455–467.

Smith, B., Samuelsson, P., Wramneby, A., Rummukainen, M., 2011. A model of the coupled dynamics of climate, vegetation and terrestrial ecosystem biogeochemistry for regional applications. Tellus a: Dyn. Meteorol. Oceanogr. 63 (1), 87–106.

Smith, M.D., Wilcox, K.R., Power, S.A., Tissue, D.T., Knapp, A.K., 2017. Assessing community and ecosystem sensitivity to climate change–toward a more comparative approach. J. Veg. Sci. 28 (2), 235–237.

Soriano, A., Sala, O., 1984. Ecological strategies in a Patagonian arid steppe. Vegetatio 56 (1), 9–15.

Strohm, S., Tyson, R.C., 2012. The effect of habitat fragmentation on cyclic population dynamics: a reduction to ordinary differential equations. Theor. Ecol. 5 (4), 495–516.

Sun, S., Wang, G., 2012. The complexity of using a feedback parameter to quantify the soil moisture-precipitation relationship. J. Geophys. Res.-Atmos. 117 (D11).

Van der Valk, A.G., 2011. Origins and development of ecology. In: Philosophy of Ecology, Volume 11 in Handbook of the Philosophy of Science, pp. 25–48 (North-Holland).

Varela, Fernandez, Gyenge, Aparicio, Bruzzone, Schlichter, 2012. Physiological and morphological short-term responses to light and temperature in two Nothofagus species of Patagonia, South America. Photosyntetica 50 (4), 557–569.

Vaz, S., Martin, C.S., Eastwood, P.D., Ernande, B., Carpentier, A., Meaden, G.J., Coppin, F., 2008. Modelling species distributions using regression quantiles. J. Appl. Ecol. 45 (1), 204–217.

Volaire, F., Norton, M., 2006. Summer dormancy in perennial temperate grasses. Ann. Bot. 98 (5), 927–933.

Walter, H., 1939. Grasland, Savanne und Busch der arideren Teile Afrikas in ihrer ökologischen Bedingtheit.

Walter, H., 1971. Natural Savannahs as a Transition to the Arid Zone. Ecology of Tropical and Subtropical Vegetation. Oliver and Boyd, Edinburgh, pp. 238–265.

Walther, G.R., 2010. Community and ecosystem responses to recent climate change. Philos. Transact. Roy. Soc. B: Biol. Sci. 365 (1549), 2019–2024.

Walther, G.R., Post, E., Convey, P., Menzel, A., Parmesan, C., Beebee, T.J., Fromentin, J.M., Hoegh-Guldberg, O., Bairlein, F., 2002. Ecological responses to recent climate change. Nature 416 (6879), 389–395.

Ward, D., Wiegand, K., Getzin, S., 2013. Walter's two-layer hypothesis revisited: back to the roots! Oecologia 172 (3), 617–630.

Westoby, M., Walker, B., Noy-Meir, I., 1989. Opportunistic management for rangelands not at equilibrium. Rangel. Ecol. Manage./J. Range Manage. Arch. 42 (4), 266–274.

Wolkovich, E.M., Cook, B.I., McLauchlan, K.K., Davies, T.J., 2014. Temporal ecology in the Anthropocene. Ecol. Lett. 17 (11), 1365–1379.

Wu, D., Zhao, X., Liang, S., Zhou, T., Huang, K., Tang, B., Zhao, W., 2015. Time-lag effects of global vegetation responses to climate change. Glob. Chang. Biol. 21 (9), 3520–3531.

Wu, W., Geller, M.A., Dickinson, R.E., 2002. The response of soil moisture to long-term variability of precipitation. J. Hydrometeorol. 3 (5), 604–613.

Xu, L., Baldocchi, D.D., Tang, J., 2004. How soil moisture, rain pulses, and growth alter the response of ecosystem respiration to temperature. Glob. Biogeochem. Cycles 18 (4).

Yoo, C., Jung, K.S., Kim, T.W., 2005. Rainfall frequency analysis using a mixed gamma distribution: evaluation of the global warming effect on daily rainfall. Hydrol. Proc.: Intern. J. 19 (19), 3851–3861.

Zaldívar, J.M., Strozzi, F., Dueri, S., Marinov, D., Zbilut, J.P., 2008. Characterization of regime shifts in environmental time series with recurrence quantification analysis. Ecol. Model. 210 (1–2), 58–70.

Zeng, N., Hales, K., Neelin, J.D., 2002. Nonlinear dynamics in a coupled vegetation–atmosphere system and implications for desert–forest gradient. J. Clim. 15 (23), 3474–3487.

Zhang, T., Yu, G., Chen, Z., Hu, Z., Jiao, C., Yang, M., Li, W., 2020. Patterns and controls of vegetation productivity and precipitation-use efficiency across Eurasian grasslands. Sci. Total Environ. 741, 140204.

Zheng, Y., Han, J., Huang, Y., Fassnacht, S.R., Xie, S., Lv, E., Chen, M., 2018. Vegetation response to climate conditions based on NDVI simulations using stepwise cluster analysis for the Three-River headwaters region of China. Ecol. Indic. 92, 18–29.

Zuo, D., Han, Y., Xu, Z., Li, P., Ban, C., Sun, W., Pang, B., Peng, D., Kan, G., Zhang, R., Yang, H., 2021. Time-lag effects of climatic change and drought on vegetation dynamics in an alpine river basin of the Tibet plateau, China. J. Hydrol. 600, 126532.